Tetrahedron integration method for strongly varying functions: Application to the *GT* self-energy

Christoph Friedrich

Peter Grünberg Institut and Institute for Advanced Simulation, Forschungszentrum Jülich and JARA, 52425 Jülich, Germany

(Received 6 June 2019; revised manuscript received 31 July 2019; published 21 August 2019)

We develop a tetrahedron method for the Brillouin-zone integration of expressions that vary a lot as a function of energy. The usual tetrahedron method replaces the continuous integral over the Brillouin zone by a weighted sum over a finite number of **k** points. The weight factors are determined under the assumption that the function to be integrated be linear inside each tetrahedron, so the method works best for functions that vary smoothly over the Brillouin zone. In this paper, we describe a new method that can deal with situations where this condition is not fulfilled. Instead of weight factors, we employ weight functions, defined as piecewise cubic polynomials over energy. Since these polynomials are analytic, any function, also strongly varying ones, can be integrated accurately and piecewise analytically. The method is applied to the evaluation of the *GT* self-energy using two techniques, analytic continuation and contour deformation. (We also describe a third technique, which is a hybrid of the two. An efficient algorithm for the dilogarithm needed for analytic continuation is formulated in Appendix.) The resulting spectral functions converge very quickly with respect to the **k**-point sampling.

DOI: 10.1103/PhysRevB.100.075142

I. INTRODUCTION

In condensed-matter physics, the translational symmetry of crystalline systems leads to the existence of vectorial quantum numbers, the Bloch vectors [1], defined to lie in the Brillouin zone, the first reciprocal unit cell. If an observable commutes with the lattice translations, its representation is diagonal in **k**, as is the case with the single-particle Hamiltonian. As a result, its eigenfunctions $\varphi^\sigma_{\mathbf{k}n}(\mathbf{r})$ and eigenvalues $\epsilon^\sigma_{\mathbf{k}n}$ can be classified with **k** as a quantum number, in addition to the spin quantum number σ and the band index n.

Some quantities of interest require a summation over these eigenstates, which thus involves a summation over the spin and band index, as well as an integration over **k**. This is because, in an infinite crystal, there are uncountably many Bloch vectors, **k** is a continuous variable. The simplest approach to carry out the **k** integration is to sample the Brillouin zone by a finite **k** mesh, for example, a Monkhort-Pack mesh [2], and simply sum over the respective **k** points. The finer the **k** mesh, the better the sum approaches the integral. However, for some quantities the size of the **k** mesh required to achieve sufficient convergence can become exceedingly large.

This is already clear for the relatively simple task of integrating over the energy eigenvalues to obtain the total energy of the single-particle system. This integration can be written as a sum over all states, and the corresponding **k** integrand would be $f^\sigma_{\mathbf{k}n}\epsilon^\sigma_{\mathbf{k}n}$ with the occupation number $f^\sigma_{\mathbf{k}n}$, which, in the zero temperature limit, changes abruptly from 1 to 0 at the Fermi energy. So, if, for some **k**, the single-particle energy $\epsilon^\sigma_{n\mathbf{k}}$ is slightly below the Fermi energy, this state would be included completely in the sum $\frac{1}{N}\sum_{\mathbf{k}} f^\sigma_{\mathbf{k}n}\epsilon^\sigma_{\mathbf{k}n}$, whereas, if **k** is chosen only slightly differently, $\epsilon^\sigma_{\mathbf{k}n}$ might happen to lie just above the Fermi energy, and the state would be excluded. It is clear that some kind of interpolation scheme that samples the Fermi surface to a certain degree would be helpful in this case.

The tetrahedron method [3] provides such a three-dimensional interpolation in reciprocal space. It divides the Brillouin-zone volume into $6N$ tetrahedra, where N is the number of **k** points (preferably) of an equidistant set of **k** points. Let us assume that we know the values of a **k**-dependent function at all corners of a given tetrahedron. Then there is a unique linear interpolation of the function inside the tetrahedron, which, since the tetrahedra fill up the whole Brillouin zone, defines the function everywhere in reciprocal space. For example, the energy eigenvalues $\epsilon^\sigma_{\mathbf{k}n}$ can be interpolated in this way, allowing the Fermi surface to be sampled accurately.

Coming back to the example above, this enables an analytic integration of $f^\sigma_{\mathbf{k}n}\epsilon^\sigma_{\mathbf{k}n}$, yielding the exact integral (of the linearized integrand) in the form of a weighted sum $\frac{1}{N}\sum_{\mathbf{k}} w^\sigma_{\mathbf{k}n}\epsilon^\sigma_{\mathbf{k}n}$. Obviously, the occupation numbers $f^\sigma_{\mathbf{k}n}(=1$ or $0)$ have been replaced by weight factors $w^\sigma_{\mathbf{k}n}$. If an occupied (unoccupied) state $\mathbf{k}n$ is far away from the Fermi energy (to be more precise, if none of the adjacent tetrahedra is cut by the Fermi energy), then $w^\sigma_{\mathbf{k}n} = 1$ (0), otherwise $w^\sigma_{\mathbf{k}n}$ is a number between 0 and 1. It does not change abruptly at the Fermi energy, which solves the aforementioned problem. Since the integration is a linear operation, the weight factors $w^\sigma_{\mathbf{k}n}$ turn out to be independent of the function to be integrated and can be pre-calculated in a computer code and stored in memory. With these weight factors, arbitrary functions can be integrated efficiently provided that they vary sufficiently smoothly in reciprocal space, so that the linearization inside the tetrahedra is a reasonable interpolation.[1]

[1]We have to remark at this point that there are, of course, other **k** integration methods. For example, when allowing finite temperatures, one can employ the Fermi-Dirac distribution function for $f^\sigma_{\mathbf{k}n}$, which changes gradually from 1 to 0 at ϵ_F (for increasing energy). However, this approach would still not represent a viable solution for the type of integrals with strongly varying function as those discussed in the present paper. Besides, it also does not attempt to interpolate

This latter condition is, however, not always fulfilled, in particular, by functions that describe the coupling to strong many-body resonances. For example, the evaluation of electronic self-energies (*GW* [4] or *GT* approximation [5,6]) require a $\mathbf{k}$ (and thus an energy) integration of an effective interaction potential [$W(\epsilon)$ or $T(\epsilon)$], which can vary a lot as a function of energy. This is true, in particular, for the magnetic T matrix used in the *GT* self-energy, which describes renormalization effects due to the scattering of electrons with magnons. Therefore we use the *GT* self-energy as a practical example in this paper.

The integral to be evaluated can be written in the following generic form:

$$\int_{\epsilon_{\mathbf{k}}<\epsilon_{\mathrm{F}}} F_{\mathbf{k}}(\epsilon_{\mathbf{k}})d^3k\,, \tag{1}$$

where the band and spin indices are dropped for simplicity and $F_{\mathbf{k}}(\epsilon)$ is an energy-dependent function that also depends on the $\mathbf{k}$ vector. It is important to note that $\mathbf{k}$ is assumed to be continuous by virtue of the tetrahedron interpolation. Although the integrals derived in Sec. III will have different integration bounds in general (including lower bounds), we assume, for the sake of argument, the Fermi energy ϵ_{F} to be the upper bound until Sec. III.

From a pragmatic point of view, it seems natural to interpret $F_{\mathbf{k}}(\epsilon_{\mathbf{k}})$ simply as a $\mathbf{k}$ dependent function just like $\epsilon^{\sigma}_{\mathbf{k}n}$ and integrate it in the same way as above, which would give the weighted sum $\frac{1}{N}\sum_{\mathbf{k}} w_{\mathbf{k}}F_{\mathbf{k}}(\epsilon_{\mathbf{k}})$. However, since $T_{\mathbf{k}}(\epsilon)$ is assumed to vary a lot in ϵ, the above condition for *standard* tetrahedron integration (smooth integrand) would be violated. Furthermore, the *GT* self-energy is a frequency-dependent function. To take this into account, expression (1) would have to be generalized to $\Sigma(\omega) = \int_{\epsilon_{\mathbf{k}}<\epsilon_{\mathrm{F}}} F_{\mathbf{k}}(\omega-\epsilon_{\mathbf{k}})d^3k$, and the standard method would approximate $\Sigma(\omega) \approx \frac{1}{N}\sum_{\mathbf{k}} w_{\mathbf{k}}F_{\mathbf{k}}(\omega-\epsilon_{\mathbf{k}})$ (omitting a normalization factor for simplicity). The strong variation of $F_{\mathbf{k}}(\epsilon)$ would thus directly translate to an equally strong and unphysical variation of the self-energy $\Sigma(\omega)$. As a solution, we introduce a different integration method, which leads to *weight functions* $w_{\mathbf{k}}(\epsilon)$ in place of the scalar weight factors $w_{\mathbf{k}}$. The $\mathbf{k}$ integral is then approximated by $\frac{1}{N}\sum_{\mathbf{k}}\int_{-\infty}^{\epsilon_{\mathrm{F}}} w_{\mathbf{k}}(\epsilon)F_{\mathbf{k}}(\epsilon)d\epsilon$ [or, including the frequency dependence, $\Sigma(\omega) = \frac{1}{N}\sum_{\mathbf{k}}\int_{-\infty}^{\epsilon_{\mathrm{F}}} w_{\mathbf{k}}(\epsilon)F_{\mathbf{k}}(\omega-\epsilon)d\epsilon$]. We demonstrate that the resulting self-energy has a very smooth and physical behavior even when $F_{\mathbf{k}}(\epsilon)$ exhibits a lot of structure, which, in the case of the *GT* self-energy, is due to the presence of delta-function-like spin-wave peaks in the T matrix.

The paper is organized as follows. Section II recapitulates the standard tetrahedron method and then introduces the new method. In Sec. III, the new method is applied to the *GT* self-energy. The implementation requires also the derivation of an efficient algorithm for the dilogarithm function, discussed in Appendix B. Section V discusses illustrative results. In Sec. VI, we draw the main conclusions.

the three-dimensional dispersion of the electronic bands, unlike the tetrahedron method.

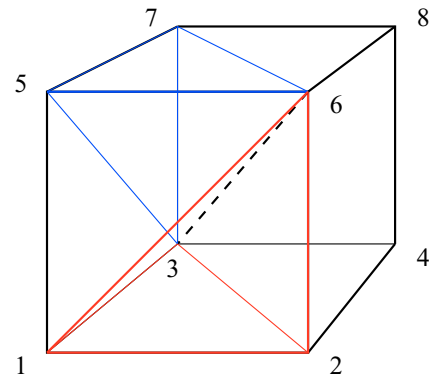

FIG. 1. Parallelepiped (cube) formed by eight adjacent $\mathbf{k}$ points (1–8) for the case of a simple cubic lattice. The six tetrahedra could have the corners (1236), (5736), (1536), (2436), (4836), and (7836). They all share the diagonal (36) of the parallelepiped (black dashed line), which can be chosen to be the one that is shortest for the given Bravais lattice. The other edges of the first two tetrahedra are shown as red and blue lines, respectively. The devision into tetrahedra is not unique.

II. TETRAHEDRON METHOD

In Sec. II A, we introduce the notation and recapitulate the standard tetrahedron method for the $\mathbf{k}$ integration over the Brillouin zone. This will set the stage for the introduction of the new method in Sec. II B.

A. Standard method

The tetrahedron method is a technique to interpolate arbitrary functions defined on a grid in $\mathbf{k}$ space in a geometrical way. It relies on a division of the Brillouin zone into $6N$ tetrahedra. Although strictly not necessary, the N $\mathbf{k}$ points are assumed to form an equidistant grid in the following for simplicity. The Brillouin zone can then be thought of as being composed of N parallelepipeds, each of which is divided into six tetrahedra in such a way that the eight $\mathbf{k}$ points forming the parallelepiped are also the tetrahedron corners. An example is shown in Fig. 1. The division into tetrahedra is not unique. It can, for example, be chosen in such a way that the edges of the tetrahedra have minimal lengths for the given geometry of the Bravais lattice, to make the tetrahedra as compact as possible.

Each tetrahedron corner coincides with one of the $\mathbf{k}$ points. A tetrahedron has four corners $\mathbf{k}_i$ ($i = 1, 2, 3, 4$), allowing a linear interpolation of a function $F_{\mathbf{k}}$ inside the tetrahedron if the function values $F_{\mathbf{k}_i}$ at the four corners are known.[2] This can be used to define the function continuously in the whole Brillouin zone and, using this interpolation, to evaluate a Brillouin-zone integral of the function analytically. The band energies are interpolated in the same way as $F_{\mathbf{k}}$, which enables a sampling of the Fermi surface by connected triangles and quadrangles. (The isoenergy surfaces in the tetrahedra have the form of triangles and quadrangles.)

[2]Throughout this paper, we use the notation $F_{\mathbf{k}}$ for values of F at discrete $\mathbf{k}$ points but also for a continuous function $F(\mathbf{k})$. It should always be clear from the context how $F_{\mathbf{k}}$ is understood.

In a first step, we assume that $\epsilon_{\mathbf{k}} < \epsilon_{\mathrm{F}}$ in the whole Brillouin zone. Then, a general $\mathbf{k}$ integral can be written as a sum over all tetrahedron contributions t

$$\frac{\Omega}{8\pi^3}\int F_{\mathbf{k}} d^3k = \frac{\Omega}{8\pi^3}\sum_t \int_t F_{\mathbf{k}} d^3k \approx \frac{\Omega}{8\pi^3}\sum_t \int_{-\infty}^{\infty} \frac{F}{b_t} S_t(F) dF, \tag{2}$$

where Ω is the unit-cell volume and $8\pi^3/\Omega$ the volume of the Brillouin zone. So, the left-hand side would be 1 if $F_{\mathbf{k}} \equiv 1$. In the last step, we have assumed $F_{\mathbf{k}}$ to be linearly approximated inside each tetrahedron (with corners $\mathbf{k}_1, \mathbf{k}_2, \mathbf{k}_3, \mathbf{k}_4$)

$$F_{\mathbf{k}} \approx F_1 + \mathbf{b}(\mathbf{k} - \mathbf{k}_1), \tag{3}$$

where $\mathbf{b}$ is the (constant) gradient $\nabla_{\mathbf{k}} F_{\mathbf{k}}$, $S(F)$ is the area of the plane of constant F inside the tetrahedron, and $F_i \equiv F_{\mathbf{k}_i}$. The index t is dropped for simplicity. Defining three vectors $\mathbf{r}_i$ $(i = 2, 3, 4)$ with $\mathbf{r}_i(\mathbf{k}_j - \mathbf{k}_1) = \delta_{ij}$, one can write $\mathbf{b} = \sum_{i=2}^{4} (F_i - F_1)\mathbf{r}_i$. Let the vectors $\mathbf{k}_i$ be ordered such that $F_1 \leqslant F_2 \leqslant F_3 \leqslant F_4$. If F is between F_1 and F_2 and $\bar{\mathbf{k}}$ the point on the plane $S(F)$ that has the minimal distance from $\mathbf{k}_1$, then $\bar{\mathbf{k}} - \mathbf{k}_1$ is perpendicular to the plane and collinear to $\mathbf{b}$ because of Eq. (3), hence $\bar{\mathbf{k}} - \mathbf{k}_1 = \alpha\mathbf{b}$ and $F - F_1 = \alpha b^2$. The partial volume of the tetrahedron defined by $F_{\mathbf{k}} \leqslant F$ is

$$\frac{(F - F_1)^3}{(F_2 - F_1)(F_3 - F_1)(F_4 - F_1)} v = \tfrac{1}{3}|\bar{\mathbf{k}} - \mathbf{k}_1| S(F) \tag{4}$$

with the tetrahedron volume v. This leads to $S(F) = a_1(F)$ with

$$a_1(F) = 3vb\frac{(F - F_1)^2}{(F_2 - F_1)(F_3 - F_1)(F_4 - F_1)} \tag{5}$$

for $F_1 \leqslant F \leqslant F_2$. Similarly, we find $S(F) = a_2(F) + a_3(F)$ for $F_2 < F < F_3$ and $S(F) = a_4(F)$ for $F_3 \leqslant F \leqslant F_4$ with

$$a_2(F) = 3vb\frac{(F - F_1)(F_4 - F)}{(F_3 - F_1)(F_4 - F_1)(F_4 - F_2)}, \tag{6}$$

$$a_3(F) = 3vb\frac{(F - F_2)(F_3 - F)}{(F_3 - F_2)(F_4 - F_2)(F_3 - F_1)}, \tag{7}$$

$$a_4(F) = 3vb\frac{(F - F_4)^2}{(F_4 - F_1)(F_4 - F_2)(F_4 - F_3)}, \tag{8}$$

see Fig. 2. The integral of Eq. (2) can now be evaluated and yields

$$\int_{-\infty}^{\infty} \frac{F}{b} S(F) dF = \frac{v}{4}(F_1 + F_2 + F_3 + F_4), \tag{9}$$

which is nothing but the arithmetic average multiplied by the tetrahedron volume. With $6Nv = 8\pi^3/\Omega$, the contribution of a given tetrahedron is

$$\frac{\Omega}{8\pi^3}\int_{-\infty}^{\infty} \frac{F}{b} S(F) dF = \frac{1}{24N}(F_1 + F_2 + F_3 + F_4). \tag{10}$$

Since each $\mathbf{k}$ point is the corner of six tetrahedra, we finally get $\frac{\Omega}{8\pi^3}\int F_{\mathbf{k}} d^3k \approx \frac{1}{N}\sum_{\mathbf{k}} w_{\mathbf{k}} F(\mathbf{k})$ with the trivial weight factors $w_{\mathbf{k}} \equiv 1$. Obviously, if $\epsilon_{\mathbf{k}} > \epsilon_{\mathrm{F}}$ in the whole Brillouin zone, then $w_{\mathbf{k}} \equiv 0$.

We now consider the case that the energy ϵ_{F} falls into the tetrahedron, i.e., $\epsilon_1 < \epsilon_{\mathrm{F}} < \epsilon_4$ with $\epsilon_i = \epsilon_{\mathbf{k}_i}$. Then, the volume

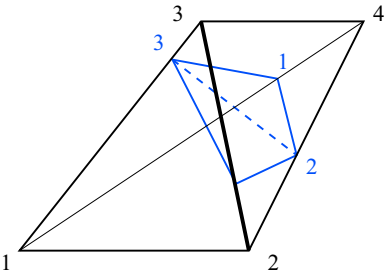

FIG. 2. Plane of constant F in a tetrahedron for the case $F_1 < F_2 < F < F_3 < F_4$. It is composed of two triangles. The corners of the first [Eq. (6)] are enumerated (blue numbers). In the other two cases ($F_1 \leqslant F \leqslant F_2$ and $F_3 \leqslant F \leqslant F_4$), the plane of constant F is a single triangle. The energies ϵ_i are interpolated in the same way.

defined by $\epsilon_{\mathbf{k}} < \epsilon_{\mathrm{F}}$ is again a tetrahedron if $\epsilon_{\mathrm{F}} \leqslant \epsilon_2$ or a combination of three tetrahedra if $\epsilon_2 < \epsilon_{\mathrm{F}} < \epsilon_4$. The corners of these new tetrahedra are obtained according to Eq. (3).[3] The integration over them is performed in the same way as above. As a consequence, the integral can be written again as a weighted sum over the $\mathbf{k}$ points

$$\frac{\Omega}{8\pi^3}\int_{\epsilon_{\mathbf{k}} < \epsilon_{\mathrm{F}}} F_{\mathbf{k}} d^3k \approx \frac{1}{N}\sum_{\mathbf{k}} w_{\mathbf{k}} F_{\mathbf{k}}. \tag{11}$$

The weight factors $w_{\mathbf{k}}$ are independent of the function $F_{\mathbf{k}}$. But now, since the condition $\epsilon_{\mathbf{k}} < \epsilon_{\mathrm{F}}$ is not fulfilled in the whole Brillouin zone, the weights are not all identical. If ϵ_{F} falls into one of the tetrahedra of which $\mathbf{k}$ is a corner, the weight $w_{\mathbf{k}}$ will be between 0 and 1. We note that one can go beyond the linear approximation by taking into account quadratic corrections [7] in the tetrahedron method. However, these corrections, too, rely on a smooth integrand as a condition and are, therefore, insufficient for the present purpose.

B. New method

In this section, we consider the integral

$$\frac{\Omega}{8\pi^3}\int_{\epsilon_{\mathbf{k}} < \epsilon_{\mathrm{F}}} F_{\mathbf{k}}(\epsilon_{\mathbf{k}}) d^3k, \tag{12}$$

where $F_{\mathbf{k}}(\epsilon)$ is a strongly varying function in ϵ. The integrand depends on $\mathbf{k}$ implicitly through $\epsilon_{\mathbf{k}}$ but also through an explicit $\mathbf{k}$ dependence of the function F itself. The latter $\mathbf{k}$ dependence and also the one of $\epsilon_{\mathbf{k}}$ is assumed to be sufficiently smooth over the Brillouin zone. We assume that, for each $\mathbf{k}$ point (of the $\mathbf{k}$-point set), the function $F_{\mathbf{k}}(\epsilon)$ is known on a dense energy mesh (or as an analytic function, e.g., a Padé approximant). So, the explicit $\mathbf{k}$ dependence is discrete, while the energy dependence can be regarded as continuous. We note in passing that the same method introduced here can be used for the more general integral $\int_{\epsilon_{\mathbf{k}} < \epsilon_{\mathrm{F}}} F_{\mathbf{k}}(f_{\mathbf{k}}) d^3k$ with an arbitrary (but smoothly varying) function $f_{\mathbf{k}}$. For clarity, we restrict ourselves to the other simpler case, which is also the relevant one for the GT self-energy.

[3] In the case $\epsilon_{\mathrm{F}} < \epsilon_2$, for example, the new corners would be at $(\mathbf{k}_1, \mathbf{k}_i', i = 2, 3, 4)$ with $\mathbf{k}_i' - \mathbf{k}_1 = \frac{\epsilon_{\mathrm{F}} - \epsilon_1}{\epsilon_i - \epsilon_1}(\mathbf{k}_i - \mathbf{k}_1)$ as obtained from $\mathbf{k}_i' - \mathbf{k}_1 = \beta(\mathbf{k}_i - \mathbf{k}_1)$ $(0 < \beta < 1)$ and $\epsilon_{\mathrm{F}} - \epsilon_1 = \mathbf{b}(\mathbf{k}_i' - \mathbf{k}_1) = \beta\mathbf{b}(\mathbf{k}_i - \mathbf{k}_1) = \beta(\epsilon_i - \epsilon_1)$.

The criterion of a "sufficiently smooth $\mathbf{k}$ dependence of the function $F_\mathbf{k}(\epsilon)$" requires some explanatory words, since we talk here about a *function of functions*: for each $\mathbf{k}$ (continuously defined), there is a function $F_\mathbf{k}(\epsilon)$ of ϵ. Firstly, the criterion does *not* mean that $F_\mathbf{k}(\epsilon)$ depends weakly on $\mathbf{k}$ for any fixed ϵ because this would be in conflict with allowing $F_\mathbf{k}(\epsilon)$ to be a strongly varying function in ϵ.[4] It might best be explained by picturing plots of $F_\mathbf{k}(\epsilon)$ for several slightly different $\mathbf{k}$ points (e.g., along a direction in $\mathbf{k}$ space). These plots should show a smooth transition from one $\mathbf{k}$ point to the next, which would allow for peaks to shift, to increase and decrease, for features to form and disappear etc. As a more mathematical definition, one could demand integrals of the form $\int w(\epsilon)F_\mathbf{k}(\epsilon)d\epsilon$ to show a weak $\mathbf{k}$ dependence, where $w(\epsilon)$ is a weight function, e.g., of the type we are going to derive, that is nonzero in a finite energy range with a smooth switching-on and -off behavior at the boundaries. In this sense, the criterion of a "sufficiently smooth $\mathbf{k}$ dependence of the function $F_\mathbf{k}(\epsilon)$" is a rather weak one, which just excludes unphysical pathologies that could not be captured with a finite $\mathbf{k}$-point set.

As already mentioned in the introduction, we could formally interpret $F_\mathbf{k}(\epsilon_\mathbf{k})$ as the function $F_\mathbf{k}$ of Eq. (11) and just use the weighted sum with the precalculated weight factors, but, due to the assumed strong variation of $F_\mathbf{k}(\epsilon)$, such an approach would be very inaccurate. Therefore, we formulate an alternative tetrahedron integration method, which will allow the strong variations of $F_\mathbf{k}(\epsilon)$ to be smoothly integrated over.

To this end, we rewrite the integral as an integral over ϵ similarly to Eq. (2)

$$\frac{\Omega}{8\pi^3}\int_{\epsilon_\mathbf{k}<\epsilon_\mathrm{F}} F_\mathbf{k}(\epsilon_\mathbf{k})d^3k \approx \frac{\Omega}{8\pi^3}\sum_t \int_{-\infty}^{\epsilon_\mathrm{F}} \frac{1}{b_t}\left[\int_{S_t(\epsilon)} F_\mathbf{k}(\epsilon)d^2k\right]d\epsilon\,. \tag{13}$$

The $\mathbf{k}$ dependence of F forces us to keep the explicit integral over the isoenergy surface $S_t(\epsilon)$, which forms a triangle or a quadrangle (i.e., two triangles, see Fig. 2). We now treat $F_\mathbf{k}(\epsilon)$ as if it were a smoothly varying scalar function $F_\mathbf{k}$, ignoring the ϵ dependence for a while. Then, the integral over a triangle can be evaluated by linearization of $F_\mathbf{k}$, which, by analogy to Eq. (9), yields the arithmetic average

$$\int_a F_\mathbf{k} d^2k = \frac{a}{3}[F_1' + F_2' + F_3'] \tag{14}$$

with the triangle area a and the triangle corners $\mathbf{k}_1'$, $\mathbf{k}_2'$, and $\mathbf{k}_3'$ with $F_i' = F_{\mathbf{k}_i'}$. We first relate the function values $F_i' = F_{\mathbf{k}_i'}$ at the triangle corners to the ones at the tetrahedron corners, $F_i \equiv F_{\mathbf{k}_i}$. Any $\mathbf{k}_i'$ lies on one of the edges of the tetrahedron (see Fig. 2). So, using linearization for $F_\mathbf{k}$ and $\epsilon_\mathbf{k}$, we have $F_i' = [(\epsilon-\epsilon_k)F_j + (\epsilon_j-\epsilon)F_k]/(\epsilon_j-\epsilon_k)$ if $\mathbf{k}_i'$ is on the edge connecting $\mathbf{k}_j$ and $\mathbf{k}_k$. Now, we reintroduce the ϵ dependence simply by the substitutions $F_i \to F_i(\epsilon)$ and $F_i' \to F_i'(\epsilon)$ in Eq. (14), thus exploiting the assumed weak dependence of $F_\mathbf{k}(\epsilon)$ on $\mathbf{k}$. And we also substitute a by the corresponding formula from Eqs. (5)–(8) (with ϵ instead of F).

Now, we have all ingredients to rewrite the right-hand side of Eq. (13). Obviously, the functions $F_i(\epsilon)$ appear linearly, so we can factor them out and write

$$\frac{\Omega}{8\pi^3}\frac{1}{b_t}\int_{S_t(\epsilon)} F_\mathbf{k}(\epsilon)d^2k \approx \sum_i w_i(\epsilon)F_i(\epsilon)\,, \tag{15}$$

with the energy-dependent *tetrahedron weight functions*

$$w_1(\epsilon) = \frac{1}{6}\begin{cases} \frac{(\epsilon-\epsilon_1)^2}{(\epsilon_2-\epsilon_1)(\epsilon_3-\epsilon_1)(\epsilon_4-\epsilon_1)}\left(\frac{\epsilon_2-\epsilon}{\epsilon_2-\epsilon_1}+\frac{\epsilon_3-\epsilon}{\epsilon_3-\epsilon_1}+\frac{\epsilon_4-\epsilon}{\epsilon_4-\epsilon_1}\right) & \text{for } \epsilon_1 \leqslant \epsilon \leqslant \epsilon_2 \\ \frac{(\epsilon-\epsilon_1)(\epsilon_4-\epsilon)}{(\epsilon_3-\epsilon_1)(\epsilon_4-\epsilon_1)(\epsilon_4-\epsilon_2)}\left(\frac{\epsilon_3-\epsilon}{\epsilon_3-\epsilon_1}+\frac{\epsilon_4-\epsilon}{\epsilon_4-\epsilon_1}\right)+\frac{(\epsilon-\epsilon_2)(\epsilon_3-\epsilon)}{(\epsilon_3-\epsilon_2)(\epsilon_4-\epsilon_2)(\epsilon_3-\epsilon_1)}\frac{\epsilon_3-\epsilon}{\epsilon_3-\epsilon_1} & \text{for } \epsilon_2 < \epsilon < \epsilon_3, \\ \frac{(\epsilon-\epsilon_4)^2}{(\epsilon_4-\epsilon_1)(\epsilon_4-\epsilon_2)(\epsilon_4-\epsilon_3)}\frac{\epsilon_4-\epsilon}{\epsilon_4-\epsilon_1} & \text{for } \epsilon_3 \leqslant \epsilon \leqslant \epsilon_4 \end{cases} \tag{16}$$

$$w_2(\epsilon) = \frac{1}{6}\begin{cases} \frac{(\epsilon-\epsilon_1)^2}{(\epsilon_2-\epsilon_1)(\epsilon_3-\epsilon_1)(\epsilon_4-\epsilon_1)}\frac{\epsilon-\epsilon_1}{\epsilon_2-\epsilon_1} & \text{for } \epsilon_1 \leqslant \epsilon \leqslant \epsilon_2 \\ \frac{(\epsilon-\epsilon_1)(\epsilon_4-\epsilon)}{(\epsilon_3-\epsilon_1)(\epsilon_4-\epsilon_1)(\epsilon_4-\epsilon_2)}\frac{\epsilon_4-\epsilon}{\epsilon_4-\epsilon_2}+\frac{(\epsilon-\epsilon_2)(\epsilon_3-\epsilon)}{(\epsilon_3-\epsilon_2)(\epsilon_4-\epsilon_2)(\epsilon_3-\epsilon_1)}\left(\frac{\epsilon_3-\epsilon}{\epsilon_3-\epsilon_2}+\frac{\epsilon_4-\epsilon}{\epsilon_4-\epsilon_2}\right) & \text{for } \epsilon_2 < \epsilon < \epsilon_3, \\ \frac{(\epsilon-\epsilon_4)^2}{(\epsilon_4-\epsilon_1)(\epsilon_4-\epsilon_2)(\epsilon_4-\epsilon_3)}\frac{\epsilon_4-\epsilon}{\epsilon_4-\epsilon_2} & \text{for } \epsilon_3 \leqslant \epsilon \leqslant \epsilon_4 \end{cases} \tag{17}$$

$$w_3(\epsilon) = \frac{1}{6}\begin{cases} \frac{(\epsilon-\epsilon_1)^2}{(\epsilon_2-\epsilon_1)(\epsilon_3-\epsilon_1)(\epsilon_4-\epsilon_1)}\frac{\epsilon-\epsilon_1}{\epsilon_3-\epsilon_1} & \text{for } \epsilon_1 \leqslant \epsilon \leqslant \epsilon_2 \\ \frac{(\epsilon-\epsilon_1)(\epsilon_4-\epsilon)}{(\epsilon_3-\epsilon_1)(\epsilon_4-\epsilon_1)(\epsilon_4-\epsilon_2)}\frac{\epsilon-\epsilon_1}{\epsilon_3-\epsilon_1}+\frac{(\epsilon-\epsilon_2)(\epsilon_3-\epsilon)}{(\epsilon_3-\epsilon_2)(\epsilon_4-\epsilon_2)(\epsilon_3-\epsilon_1)}\left(\frac{\epsilon-\epsilon_1}{\epsilon_3-\epsilon_1}+\frac{\epsilon-\epsilon_2}{\epsilon_3-\epsilon_2}\right) & \text{for } \epsilon_2 < \epsilon < \epsilon_3, \\ \frac{(\epsilon-\epsilon_4)^2}{(\epsilon_4-\epsilon_1)(\epsilon_4-\epsilon_2)(\epsilon_4-\epsilon_3)}\frac{\epsilon_4-\epsilon}{\epsilon_4-\epsilon_3} & \text{for } \epsilon_3 \leqslant \epsilon \leqslant \epsilon_4 \end{cases} \tag{18}$$

$$w_4(\epsilon) = \frac{1}{6}\begin{cases} \frac{(\epsilon-\epsilon_1)^2}{(\epsilon_2-\epsilon_1)(\epsilon_3-\epsilon_1)(\epsilon_4-\epsilon_1)}\frac{\epsilon-\epsilon_1}{\epsilon_4-\epsilon_1} & \text{for } \epsilon_1 \leqslant \epsilon \leqslant \epsilon_2 \\ \frac{(\epsilon-\epsilon_1)(\epsilon_4-\epsilon)}{(\epsilon_3-\epsilon_1)(\epsilon_4-\epsilon_1)(\epsilon_4-\epsilon_2)}\left(\frac{\epsilon-\epsilon_1}{\epsilon_4-\epsilon_1}+\frac{\epsilon-\epsilon_2}{\epsilon_4-\epsilon_2}\right)+\frac{(\epsilon-\epsilon_2)(\epsilon_3-\epsilon)}{(\epsilon_3-\epsilon_2)(\epsilon_4-\epsilon_2)(\epsilon_3-\epsilon_1)}\frac{\epsilon-\epsilon_2}{\epsilon_4-\epsilon_2} & \text{for } \epsilon_2 < \epsilon < \epsilon_3, \\ \frac{(\epsilon-\epsilon_4)^2}{(\epsilon_4-\epsilon_1)(\epsilon_4-\epsilon_2)(\epsilon_4-\epsilon_3)}\left(\frac{\epsilon-\epsilon_1}{\epsilon_4-\epsilon_1}+\frac{\epsilon-\epsilon_2}{\epsilon_4-\epsilon_2}+\frac{\epsilon-\epsilon_3}{\epsilon_4-\epsilon_3}\right) & \text{for } \epsilon_3 \leqslant \epsilon \leqslant \epsilon_4 \end{cases} \tag{19}$$

and $w_i(\epsilon) = 0$ elsewhere. The weight functions are independent of $F_\mathbf{k}(\epsilon)$ and piecewise cubic polynomials over ϵ. Following the tetrahedron construction, these weight functions are assigned to the respective $\mathbf{k}$ points. Each $\mathbf{k}$ point gets contributions from all adjacent (six) tetrahedra, which are summed to an effective weight function $w_\mathbf{k}(\epsilon)$, now indexed with $\mathbf{k}$. Equation (13) can

[4] As a trivial example, consider k to be a one-dimensional parameter and suppose a weak functional k dependence of the form $F_k(\epsilon) = F(\epsilon + k)$. Then the function $k \mapsto F_k(\epsilon)$ would show the same strong variations as $\epsilon \mapsto F_k(\epsilon)$.

then be written as

$$\frac{\Omega}{8\pi^3}\int_{\epsilon_{\mathbf{k}}<\epsilon_{\mathrm{F}}} F_{\mathbf{k}}(\epsilon_{\mathbf{k}})d^3k \approx \frac{1}{N}\sum_{\mathbf{k}}\int_{-\infty}^{\epsilon_{\mathrm{F}}} w_{\mathbf{k}}(\epsilon)F_{\mathbf{k}}(\epsilon)d\epsilon\,, \quad (20)$$

which is the desired result. To keep the polynomial coefficients numerically small, it is recommendable to define the polynomials with respect to the relative value $\epsilon-\epsilon_{\mathbf{k}}$ instead of the absolute value ϵ. Note that the simple $\mathbf{k}$ summation (discussed in the introduction) is recovered if we set $w_{\mathbf{k}}(\epsilon)=\delta(\epsilon-\epsilon_{\mathbf{k}})$.

Each weight function $w_{\mathbf{k}}(\epsilon)$ integrates to 1. Remember that, in the standard method, we have $w_{\mathbf{k}}=1$ if neither of the tetrahedra adjacent to $\mathbf{k}$ are cut by the Fermi energy ϵ_{F}, and otherwise $0<w_{\mathbf{k}}<1$. In the present case, the functions $w_{\mathbf{k}}(\epsilon)$ are independent of ϵ_{F}. The energy ϵ_{F} is, instead, taken into account as the upper integration bound. In this sense, the weight functions are more general than the weight factors of Sec. II A because they do not depend on ϵ_{F}, unlike $w_{\mathbf{k}}$. This will be helpful in Sec. III, where the upper bound will take the role of a variable quantity dependent on the argument of the self-energy. In addition to ϵ_{F}, we will then also have to introduce a lower integration bound.

If $F_{\mathbf{k}}(\epsilon)$ is defined on an energy mesh $\{\epsilon_\nu\}$, the integrations can be performed piecewise analytically assuming linear interpolation between the mesh points, since the $w_{\mathbf{k}}(\epsilon)$ are just cubic polynomials. Also, products of polynomials with more complex functions [we will later need to consider multiplication with the complex logarithm] can be performed analytically.

To validate Eqs. (16)–(19), it is interesting to consider slowly varying functions $F_i(\epsilon)$, in which case the results of Sec. II A should be recovered. If $F_i(\epsilon)$ is constant, each tetrahedron corner ($i=1,2,3,4$) contributes

$$\int_{\epsilon_1}^{\epsilon_4} w_i(\epsilon)d\epsilon = \frac{1}{24}\,. \quad (21)$$

So, each corner "represents" one fourth of the tetrahedron (which takes up one sixth of the parallelepiped, so $4\times 6=24$), as expected from Eq. (10). We can say that the contribution of a tetrahedron corner is "spread" over the interval $[\epsilon_1,\epsilon_4]$. Using the (linear) function $F_i(\epsilon)=\epsilon$, we would get

$$\int_{\epsilon_1}^{\epsilon_4} \epsilon\, w_i(\epsilon)d\epsilon = \frac{1}{120}\left(\epsilon_i+\sum_{j=1}^{4}\epsilon_j\right). \quad (22)$$

The contributions of the tetrahedron corners to the total integral are not equal. The energy value at the ith corner gets twice as much weight (1/60) as the other values (1/120). This seems to contradict Eq. (10) of the standard method, in which all weights are identically 1/24. But it should be remembered that Eq. (10) already represents the integration over the whole tetrahedron. In the present case, this would amount to summing over all corners, which then yields the expected result

$$\sum_{i=1}^{4}\int_{\epsilon_1}^{\epsilon_4} \epsilon\, w_i(\epsilon)d\epsilon = \frac{1}{24}\sum_{i=1}^{4}\epsilon_i\,, \quad (23)$$

i.e., each tetrahedron corner contributes the same as in the standard method.

It can be shown that if $\epsilon_1<\epsilon_2<\epsilon_3<\epsilon_4$, $w_i(\epsilon)$ and the derivatives $w_i'(\epsilon)$ are continuous, $w_i''(\epsilon)$ is continuous except at ϵ_i, and $w_i'''(\epsilon)$ is discontinuous. (Note that $w_i(\epsilon)=0$ if $\epsilon\leqslant\epsilon_1$ or $\epsilon\geqslant\epsilon_4$.) If $\epsilon_i=\epsilon_{i+1}$, then $w_i'(\epsilon)$ and $w_{i+1}'(\epsilon)$ are discontinuous at ϵ_i. If $\epsilon_i=\epsilon_{i+1}=\epsilon_{i+2}$, then $w_i(\epsilon)$, $w_{i+1}(\epsilon)$, and $w_{i+2}(\epsilon)$ are discontinuous at ϵ_i. Figure 3 shows $w_i(\epsilon)$ and the derivatives $w_2^{(\nu)}(\epsilon)$ (scaled by 24) for the case $\epsilon_i\equiv i$. Due to symmetry, $w_1(\epsilon)=w_4(5-\epsilon)$ and $w_2(\epsilon)=w_3(5-\epsilon)$. The curves $w_i(\epsilon)$ are very smooth, discontinuities appear only in the second derivative.

III. SELF-ENERGY

In this section, we discuss the evaluation of the electronic self-energy with the help of the tetrahedron method discussed before. We use here a generic form of the self-energy

$$\Sigma(\mathbf{r},\mathbf{r}';\omega)=\frac{1}{2\pi\mathrm{i}}\int_{-\infty}^{\infty} G(\mathbf{r},\mathbf{r}';\omega+\omega')T(\mathbf{r},\mathbf{r}';-\omega')d\omega'\,, \quad (24)$$

where G is the Green function and T an effective interaction potential. The latter can be the T matrix but also $-W$, the negative of the screened interaction W, used in the GW approximation [4]. The spin dependence is omitted for simplicity, as it is irrelevant for the present purpose. (In the case of GW, Σ and G would have the same and W no spin index. In the case of magnetic GT, Σ and G would have opposite indices, σ and $\sigma'=-\sigma$, and the T matrix the index pair $\sigma\sigma'$.)

After insertion of the Lehmann representation of the Green function

$$G(\mathbf{r},\mathbf{r}';\omega)=\frac{\Omega}{8\pi^3}\int d^3k\sum_n \frac{\varphi_{\mathbf{k}n}(\mathbf{r})\varphi_{\mathbf{k}n}^*(\mathbf{r}')}{\omega-\epsilon_{n\mathbf{k}}+\mathrm{i}\eta\,\mathrm{sgn}(\epsilon_{\mathbf{k}n}-\epsilon_{\mathrm{F}})}\,, \quad (25)$$

where η is a positive infinitesimal, the expectation value of the self-energy becomes

$$\langle\varphi_{\mathbf{q}m}|\Sigma(\omega)|\varphi_{\mathbf{q}m}\rangle=\frac{1}{2\pi\mathrm{i}}\frac{\Omega}{8\pi^3}\int d^3k\sum_n\int_{-\infty}^{\infty}d\omega' \times\frac{T_{\mathbf{q}m,\mathbf{k}n}(-\omega')}{\omega+\omega'-\epsilon_{\mathbf{k}n}+\mathrm{i}\eta\,\mathrm{sgn}(\epsilon_{\mathbf{k}n}-\epsilon_{\mathrm{F}})}. \quad (26)$$

The quantity $T_{\mathbf{q}m,\mathbf{k}n}(\omega)$ can be quite complex. In the case of magnetic GT, it is the matrix element of the four-point T matrix $[T^{\sigma\sigma'}(\mathbf{r}_1,\mathbf{r}_2,\mathbf{r}_3,\mathbf{r}_4;\omega)]$ with respect to the wave-function pairs $\varphi_{\mathbf{k}n}^{\sigma'}(\mathbf{r}_1)\varphi_{\mathbf{q}m}^{\sigma\,*}(\mathbf{r}_2)$ and $\varphi_{\mathbf{k}n}^{\sigma'*}(\mathbf{r}_3)\varphi_{\mathbf{q}m}^{\sigma}(\mathbf{r}_4)$ [6]. In the case of GW, it is the matrix element of the two-point screened interaction W $[W(\mathbf{r}_1,\mathbf{r}_2;\omega)]$ with respect to the products $\varphi_{\mathbf{k}n}(\mathbf{r}_1)\varphi_{\mathbf{q}m}^*(\mathbf{r}_1)$ and $\varphi_{\mathbf{k}n}^*(\mathbf{r}_2)\varphi_{\mathbf{q}m}(\mathbf{r}_2)$ [8]. For the present purpose, we only need to know that it is defined for each $\mathbf{k}$ point of the $\mathbf{k}$ mesh as a function of ω. For simplicity, we restrict ourselves to the diagonal elements [Eq. (26)]. The generalization to off-diagonal elements $\langle\varphi_{\mathbf{q}m}|\Sigma(\omega)|\varphi_{\mathbf{q}m'}\rangle$ is straightforward.

We discuss two ways of evaluating Eq. (26), *analytic continuation* (AC) [9,10] and *contour deformation* (CD) [11,12]. (The acronyms will refer to the methods in the following, not to the mathematical concepts). In the former approach, one employs a formulation on the imaginary frequency axis

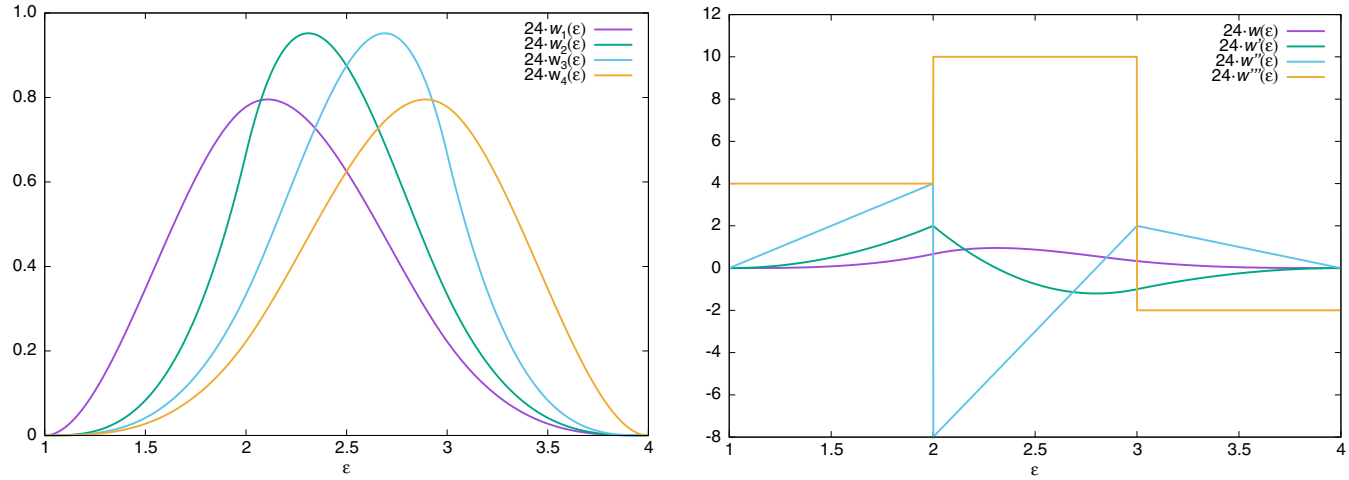

FIG. 3. (Left) The weight functions $w_i(\epsilon)$ for $\epsilon_i = i$; (right) the derivatives $w_2^{(\nu)}(\epsilon)$ ($\nu = 0, 1, 2, 3$); all functions are scaled by 24, so the area under each curve (left) is 1.

($\omega \to \mathrm{i}\omega$ and $\omega' \to \mathrm{i}\omega'$), which requires a subsequent analytic continuation of the self-energy to the real frequency axis, often carried out with Padé approximants [13]. In the second approach (CD), the frequency convolution of Eq. (26) is performed explicitly, which yields the self-energy directly for real frequencies, thus eliminating the need for the often ill-conditioned Padé extrapolation used in AC. We discuss both techniques in the following, in particular, in relation to the integration method introduced in Sec. II B.

A. Contour deformation

The CD method relies on the interpretation of the frequency convolution in Eq. (24) as an integral along a closed integration contour, namely from $-\infty$ to ∞ along the real axis, and then back to $-\infty$ along a semiarc of infinite radius over the positive complex half-plane. The integral along the semiarc is zero because the integrand behaves as $\propto \omega^{-2}$. According to the residue theorem, deforming this contour path does not change the integrated value as long as the new contour encloses the same poles [of $G(\omega + \omega')$ and $T(-\omega')$]. We can exploit this freedom to define an integration path that avoids, as best as possible, the strong variation of $T(-\omega')$ along the real frequency axis. Such a path is shown in Fig. 4. The integral from $-\mathrm{i}\infty$ to $\mathrm{i}\infty$ along the imaginary axis gives a nonvanishing contribution. Between 0 and $i\eta$ (in the case $\omega < \epsilon_F$) we have to take a rectangular detour (of infinitesimal height $\mathrm{i}\eta$) to enclose the poles coming from $G(\omega + \omega')$. Fortunately, poles from $T(-\omega')$ do not fall inside the rectangle, so that we can integrate around it analytically by summing up the residues coming from the Green-function poles. The integration path can then be regarded as consisting of two parts, an integration along the imaginary axis (from $-\mathrm{i}\infty$ to $\mathrm{i}\infty$) and the integration around the rectangle. The case $\omega > \epsilon_F$ can be treated analogously. The resulting self-energy expression reads

$$\langle\varphi_{\mathbf{q}m}|\Sigma(\omega)|\varphi_{\mathbf{q}m}\rangle = \frac{1}{2\pi}\frac{\Omega}{8\pi^3}\sum_n \int d^3k \int_{-\infty}^{\infty} d\omega' \frac{T_{\mathbf{q}m,\mathbf{k}n}(-\mathrm{i}\omega')}{\omega + \mathrm{i}\omega' - \epsilon_{\mathbf{k}n}} + \frac{\Omega}{8\pi^3}\begin{cases} \sum_n \int_{\omega<\epsilon_{\mathbf{k}n}<\epsilon_\mathrm{F}} T_{\mathbf{q}m,\mathbf{k}n}(\omega - \epsilon_{\mathbf{k}n})\, d^3k & \text{for } \omega < \epsilon_\mathrm{F} \\ -\sum_n \int_{\epsilon_\mathrm{F}<\epsilon_{\mathbf{k}n}<\omega} T_{\mathbf{q}m,\mathbf{k}n}(\omega - \epsilon_{\mathbf{k}n})\, d^3k & \text{for } \omega > \epsilon_\mathrm{F} \end{cases}, \tag{27}$$

where the n summation in the first term is over infinitely many bands, while the one of the second term (the "rectangle") is finite by virtue of the $\mathbf{k}$ integration bounds.

The function $T_{\mathbf{q}m,\mathbf{k}n}$ is given on a mesh $\{\mathrm{i}\omega_\mu\}$ along the imaginary axis. Due to the symmetry $T_{\mathbf{q}m,\mathbf{k}n}(-\mathrm{i}\omega) = T^*_{\mathbf{q}m,\mathbf{k}n}(\mathrm{i}\omega)$ [or $W_{\mathbf{q}m,\mathbf{k}n}(-\mathrm{i}\omega) = W_{\mathbf{q}m,\mathbf{k}n}(\mathrm{i}\omega)$], the mesh needs to include only positive ω_μ. To evaluate the integral of the first term, it is recommendable to interpolate the numerator in such a way that an analytic frequency integration is possible, for example, using Padé approximants [also see Eqs. (28) and (29)]. The result has the form $F_\mathbf{k}$ of Sec. II A or, if written as a function of energy, $F_\mathbf{k}(\epsilon_\mathbf{k})$ of Sec. II B. Along the imaginary axis, the function is usually smooth enough to be dealt with adequately using the standard method, but, as we will show later, treating the first term with the new method leads to more accurate results and, as a consequence, to a much better $\mathbf{k}$-point convergence. The respective integrals can be evaluated with elementary functions. The derivation is however quite involved. We discuss it in detail in Appendix A.

The problematic term, however, and the one that forced us to develop the new integration method, is the second term because its integrand is a strongly varying function. Using the standard method with $T_{\mathbf{q}m,\mathbf{k}n}(\omega - \epsilon_{\mathbf{k}n})$ for $F_\mathbf{k}$ in the weighted sum, Eq. (11) with suitably adjusted integration

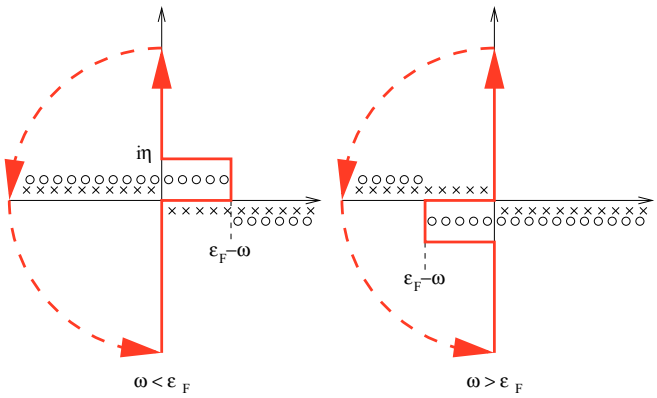

FIG. 4. The red lines show the integration contour used in the contour deformation technique to evaluate Eq. (24). The dashed lines (quarter arcs of infinite radius) do not contribute to the integral. The circles and crosses represent the poles of $G(\omega+\omega')$ and $T(-\omega')$, respectively. By inspection, the residues included in the integration path from $-\infty$ to $-\mathrm{i}\infty$, then to $\mathrm{i}\infty$, and back to $-\infty$ are the same as in a contour from $-\infty$ to ∞, and then back to $-\infty$ along a semiarc of infinite radius over the positive complex half-plane.

bounds, would therefore lead to an equally strongly varying self-energy. Such a self-energy is unphysical because the $\mathbf{k}$ integration is expected to integrate over the strong variations of $T_{\mathbf{q}m,\mathbf{k}n}(\omega)$ in a smooth way and should thus produce a well behaved self-energy. Therefore we employ the new integration method. This can be done straightforwardly by interpreting $T_{\mathbf{q}m,\mathbf{k}n}(\omega-\epsilon_{\mathbf{k}n})$ as the function $F_{\mathbf{k}}(\epsilon_{\mathbf{k}})$ of Eq. (20), again with suitably adjusted integration bounds as a trivial generalization of the equation. Let us suppose that $T_{\mathbf{q}m,\mathbf{k}n}(\omega)$ is given on a mesh $\{\omega_\nu\}$ along the real frequency axis. With an interpolation between the mesh points such as linear or spline interpolation, the ϵ integrand becomes a piecewise defined polynomial allowing a straightforward analytic integration. The integral pieces consist of the combined intervals of $\{\omega_\nu\}$ and those of the weight functions $w_{\mathbf{k}}(\epsilon)$, see Sec. II B. The simple linear interpolation of $T_{\mathbf{q}m,\mathbf{k}n}(\omega)$ has proven to be sufficiently accurate in our calculations.

The CD method is computationally more demanding than AC, mostly because it requires the effective interaction potential T to be evaluated on a mesh on the real frequency axis in addition to the one on the imaginary axis. There is an alternative that can be understood as a *hybrid* of the two methods: It is based on Eq. (27) but employs an analytic continuation of $T_{\mathbf{q}m,\mathbf{k}n}$ from the imaginary to the real axis, needed for the "rectangle" term. So, $T_{\mathbf{q}m,\mathbf{k}n}$ needs to be known only on the imaginary axis, like in the AC method. It will turn out in Sec. V that the *hybrid* method is considerably faster than but similarly accurate as the standard CD approach and more stable than the AC method.

Thiele's continued fraction formula [13] (indices omitted for simplicity)

$$T(-z)=\cfrac{1}{c_1+\cfrac{z-\mathrm{i}\omega_1}{c_2+\cfrac{z-\mathrm{i}\omega_2}{c_3+\ldots}}} \tag{28}$$

with complex parameters c_μ enables an analytic continuation from the imaginary axis to the complex plane $z\in\mathbb{C}$ with $\Im z\geqslant 0$ $(\Im z>0)$ for $\Re z\geqslant 0$ $(\Re z<0)$.[5] In Eq. (28), we have employed the negative argument $-z$ on the left because of the corresponding sign in the argument of $T[-(\epsilon-\omega)]$ in Eq. (27). The complex parameters c_μ are determined from the known function values $T(-\mathrm{i}\omega_\mu)$. Determining the coefficients, instead, from $T(\mathrm{i}\omega_\mu)=T^*(-\mathrm{i}\omega_\mu)$ $[W(\mathrm{i}\omega_\mu)=W(-\mathrm{i}\omega_\mu)]$ yields a second approximant that completes the definition with the complementary domain of the complex plane. (This piecewise definition is a consequence of the pole structure of the time-ordered T and W, see Ref. [14].) In order to be able to perform the ϵ integration analytically, we rewrite Eq. (28) in the Padé form

$$T(-z)=\sum_\mu \frac{a_\mu}{z-p_\mu}\,. \tag{29}$$

The residues a_μ and poles p_μ are determined to machine precision with the Newton-Raphson technique. Note that for real $z=\omega$, there are again two different Padé formulas for $\omega\geqslant 0$ and $\omega<0$. Equation (29) then replaces the linear or spline interpolation of T discussed earlier. Fortunately, the resulting ϵ integrals appearing in Eq. (20) can easily be expressed with elementary functions, again in the form of a piecewise integration within the intervals of definition of $w_{\mathbf{k}}(\epsilon)$.

B. Analytic continuation

In the AC approach, one employs a formulation on the imaginary frequency axis, where $T_{\mathbf{q}m,\mathbf{k}n}(\mathrm{i}\omega)$ has a smooth behavior, so frequency convolutions can be carried out accurately on relatively coarse frequency meshes. The self-energy is then also defined on a mesh of imaginary frequencies, usually the same mesh,

$$\langle\varphi_{\mathbf{q}m}|\Sigma(\mathrm{i}\omega)|\varphi_{\mathbf{q}m}\rangle = \frac{1}{2\pi}\frac{\Omega}{8\pi^3}\sum_n\int d^3k\int_{-\infty}^{\infty}d\omega'\frac{T_{\mathbf{q}m,\mathbf{k}n}(-\mathrm{i}\omega')}{\mathrm{i}\omega+\mathrm{i}\omega'-\epsilon_{\mathbf{k}n}}\,. \tag{30}$$

The frequency and subsequent $\mathbf{k}$ integrations are computed in the same way as the first term of Eq. (27) with $\omega\to\mathrm{i}\omega$, see Appendix A. In order to obtain the physically relevant self-energy, an analytic continuation to the real-frequency axis has to be carried out, for which Padé approximants [13] in the form of Eqs. (28) and (29) [then $T\to\Sigma$, whose diagonal elements fulfill the symmetry $\Sigma(-\mathrm{i}\omega)=\Sigma^*(\mathrm{i}\omega)$] are often employed.

[5]The continued fraction is truncated at c_M, where M is the number of mesh points ω_μ. Equation (28) is only valid if M is even because only then does the formula behave as z^{-1}. If the number of mesh points is odd, an additional coefficient (c_{M+1}, to reach an even number of coefficients) can be fixed by imposing another constraint, e.g., for the asymptotic $\omega\to\infty$ behavior or for the gradient at $\omega=0$.

IV. COMPUTATIONAL DETAILS

We have implemented the new tetrahedron **k** integration method into the SPEX code [8] and applied it to the *GT* self-energy, Eq. (26), where the T matrix is constructed from solutions of the Bethe-Salpeter equation based on a Wannier representation [6]. The results shown in the next section are for iron, which exhibits a particularly strong electronic renormalization due to electron-magnon scattering. Core and valence electrons are treated on an equal footing within the full-potential linearized augmented-plane-wave (FLAPW) method. We will show the self-energy for selected states calculated with a $10 \times 10 \times 10$ **k**-point set and also the **q**-resolved spectral function

$$S^\sigma(\omega, \mathbf{q}) = -\frac{1}{\pi}\mathrm{sgn}(\omega - \epsilon_\mathrm{F}) \sum_m \mathrm{Im} \frac{1}{\omega - \epsilon^\sigma_{\mathbf{q}m} - \Sigma^\sigma_{\mathbf{q}m}(\omega - \Delta_v)} \quad (31)$$

(*GT*-renormalized band structure), where $\Sigma^\sigma_{\mathbf{q}m}(\omega) = \langle \varphi^\sigma_{\mathbf{q}m} | \Sigma^\sigma(\omega) | \varphi^\sigma_{\mathbf{q}m} \rangle$ and Δ_v is a parameter defined in such a way that the many-body renormalization leaves the Fermi energy unchanged [4,6]. (The parameter Δ_v can be viewed as enforcing a self-consistency condition on the self-energy.)

We note that setting $\Sigma^\sigma_{\mathbf{q}m}(\omega - \Delta_v) \equiv -i\eta\mathrm{sgn}(\omega - \epsilon_\mathrm{F})$ (with a positive infinitesimal η) would yield [according to $\mathrm{Im}(\omega \mp i\eta)^{-1} = \pm\pi\delta(\omega)$] the spectral function of the noninteracting reference system: a series of delta functions, one for each single-particle energy $\epsilon^\sigma_{\mathbf{q}m}$. The self-energies in the *GT* and *GW* approximation have nonvanishing (noninfinitesimal) real and imaginary parts, and the spectral function then becomes a smooth function of frequency. Usually, the *GW* self-energy shows only little structure over the whole frequency range of the valence and low-lying conduction states. It is then possible to solve approximately an effective single-particle equation (the quasiparticle equation) instead of calculating the spectral function of Eq. (31). The solution can be represented as a renormalized band structure that often looks very similar to the one of the noninteracting reference system. Its band energies differ from the latter by the real-part of the self-energy, and the imaginary part gives rise to a lifetime band broadening, which, at that, is often neglected. This approach proves to be inadequate for the *GT* self-energy, which shows much more structure in the relevant frequency range. We will

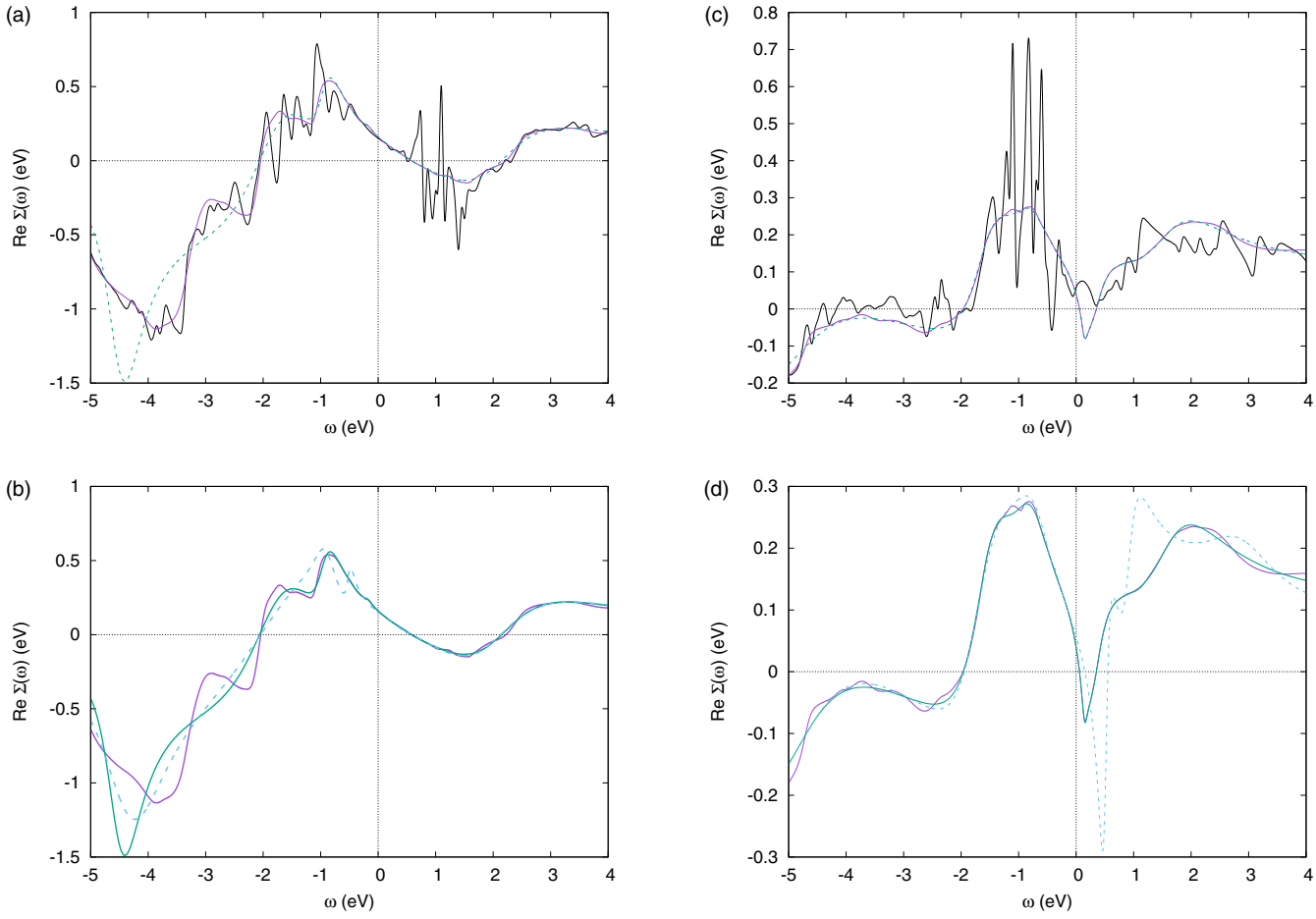

FIG. 5. Real part of self-energy for [(a) and (b)] the highest occupied spin-up and [(c) and (d)] the lowest unoccupied spin-down state at the Γ point of iron. In (a) and (c), we show the self-energy calculated with CD using the standard (black line) and the new tetrahedron method (magenta line), as well as the one calculated with AC using the new tetrahedron method (dashed green line). The magenta and green (solid) curves in (b) and (d) are the same as in (a) and (c). In addition, we show the AC self-energy calculated with the standard tetrahedron method as the blue dashed line. The frequency is with respect to the Fermi energy.

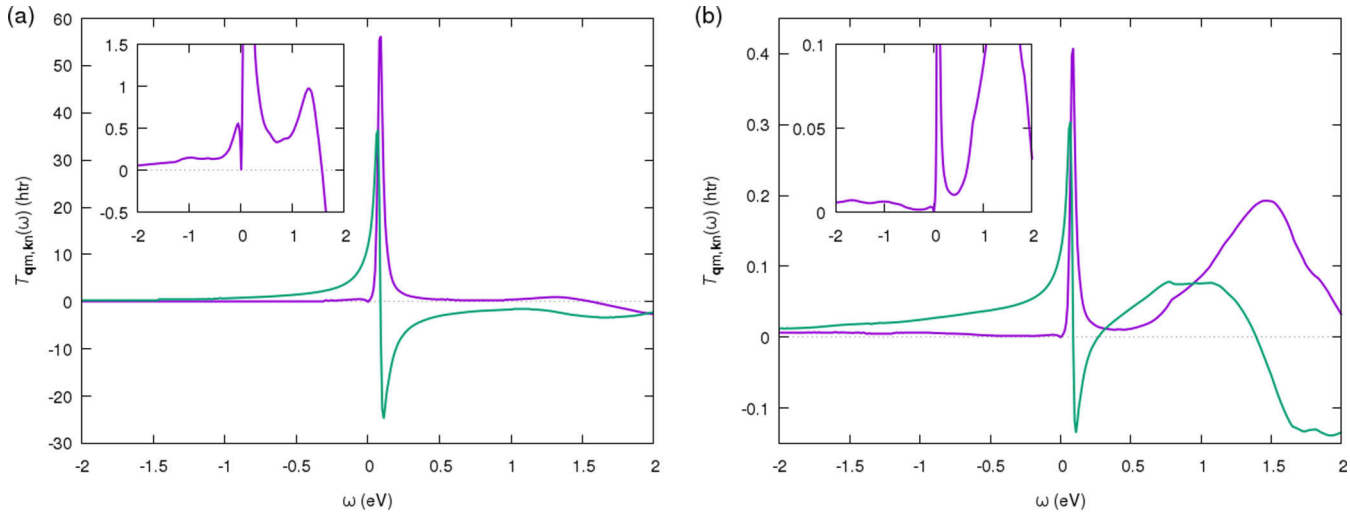

FIG. 6. T matrix elements for $\mathbf{q} = \mathbf{0}$, $\mathbf{k} = (0, 1, 1)/10$ (with respect to the reciprocal basis vectors), $m = 6$ (spin up), (a) $n = 6$ and (b) $n = 2$ (spin down). Real and imaginary components shown as green and magenta lines, respectively. The imaginary component vanishes at $\omega = 0$, see insets. The unphysical sign change of the imaginary part at around 1.5 eV (a) is due to a violation of causality [6]. The sharp peak close to $\omega = 0$ corresponds to a spin-wave excitation. The broad continuum at larger frequencies (positive and also negative, see insets) are due to Stoner excitations.

see that this can lead to a loss of quasiparticle character of the bands. For this reason, we directly evaluate Eq. (31) without resorting to a quasiparticle approximation.

Once $S^\sigma(\omega, \mathbf{q})$ has been evaluated for several $\mathbf{q}$ vectors along a high-symmetry line in the Brillouin zone, one can combine these to prepare a renormalized band structure. We have done this along a path from P over Γ to N. The spectral function was calculated for 312 $\mathbf{q}$ points along this path. We used the same parameters as detailed in Ref. [6] and considered several $\mathbf{k}$-point sets ($5 \times 5 \times 5$, $7 \times 7 \times 7$, $10 \times 10 \times 10$, and $14 \times 14 \times 14$) to investigate the $\mathbf{k}$ convergence of the renormalized band structure. The calculations were carried out on the supercomputer JURECA at the Jülich Supercomputing Centre [15].

V. RESULTS

In a first test, we have calculated the self-energy for two states, the highest occupied spin-up and the lowest unoccupied spin-down state at the Γ point of iron. Figures 5(a) and 5(c) show the real part of the self-energies as obtained with the CD technique using the standard (black line) and the new tetrahedron method (magenta line). The unphysical strong variation of the black curve is caused by the strong variation of the T matrix (Fig. 6), which, in the standard method, is not properly integrated out.

To be more precise, in the expression $\Sigma(\omega) \sim \sum_{\mathbf{k}} w_{\mathbf{k}} T_{\mathbf{k}}(\omega - \epsilon_{\mathbf{k}})$ the energies $\epsilon_{\mathbf{k}}$ are discrete numbers (since the $\mathbf{k}$-point set is discrete), so the functional form of $T_{\mathbf{k}}(\omega)$ imprints itself on the self-energy $\Sigma(\omega)$. In the new integration method, $\epsilon_{\mathbf{k}}$ is taken as a continuous variable, and the strong variations of the T matrix are properly integrated over according to $\Sigma(\omega) \sim \sum_{\mathbf{k}} \int w_{\mathbf{k}}(\epsilon) T_{\mathbf{k}}(\omega - \epsilon) d\epsilon$, producing a smooth and physical self-energy, shown as the magenta line. The magenta line has the same overall form as the black line but without exhibiting the strong fluctuations.

In addition, Figs. 5(a) and 5(c) include the self-energy as obtained from AC using the new tetrahedron method as the green dashed line. Although, as discussed before, the new tetrahedron method was implemented specifically for integrations over real frequencies, it also improves considerably the integration along the imaginary frequency axis and the subsequent analytic continuation. It is extraordinary how closely the green dashed line follows the magenta line, in particular for the spin-down self-energy [Fig. 5(c)]. The AC self-energy does show some deviations especially for large positive and negative frequencies, but one should keep in mind that, although the self-energies enter Eq. (31) with their ω dependence over the whole frequency range, the largest contributions come from frequencies around $\omega = \epsilon^\sigma_{\mathbf{q}m}$ where the denominator reduces to $\Sigma^\sigma_{\mathbf{q}m}(\omega - \Delta_v)$. We will later see that, when being used with the new tetrahedron method, the AC self-energies are generally nearly as accurate and stable as the CD self-energy, and that at a fraction of computing time.

In Figs. 5(b) and 5(d), we compare the magenta and green lines with the self-energy obtained from AC using the standard tetrahedron method (blue dashed lines). In fact, this self-energy is much less accurate than the ones calculated with the new method. It exhibits some spurious oscillations in the important frequency region close to the Fermi energy ($\omega = 0$), which will have a detrimental effect on the $\mathbf{q}$-resolved spectral functions, discussed in the following.

After having calculated $\Sigma^\sigma_{\mathbf{q}m}(\omega)$ for each state m, it is possible to evaluate Eq. (31) yielding the spectral function $S^\sigma(\omega, \mathbf{q})$ for the respective $\mathbf{q}$ point. This can be done for a number of $\mathbf{q}$ points along a line in reciprocal space, which then yields the renormalized band structure as explained in the previous section. Figures 7 and 8 present the renormalized band structures for the spin-up and spin-down channels of iron from P to Γ and Γ to N calculated with four different $\mathbf{k}$-point sets: $5 \times 5 \times 5$, $7 \times 7 \times 7$, $10 \times 10 \times 10$, and $14 \times 14 \times 14$.

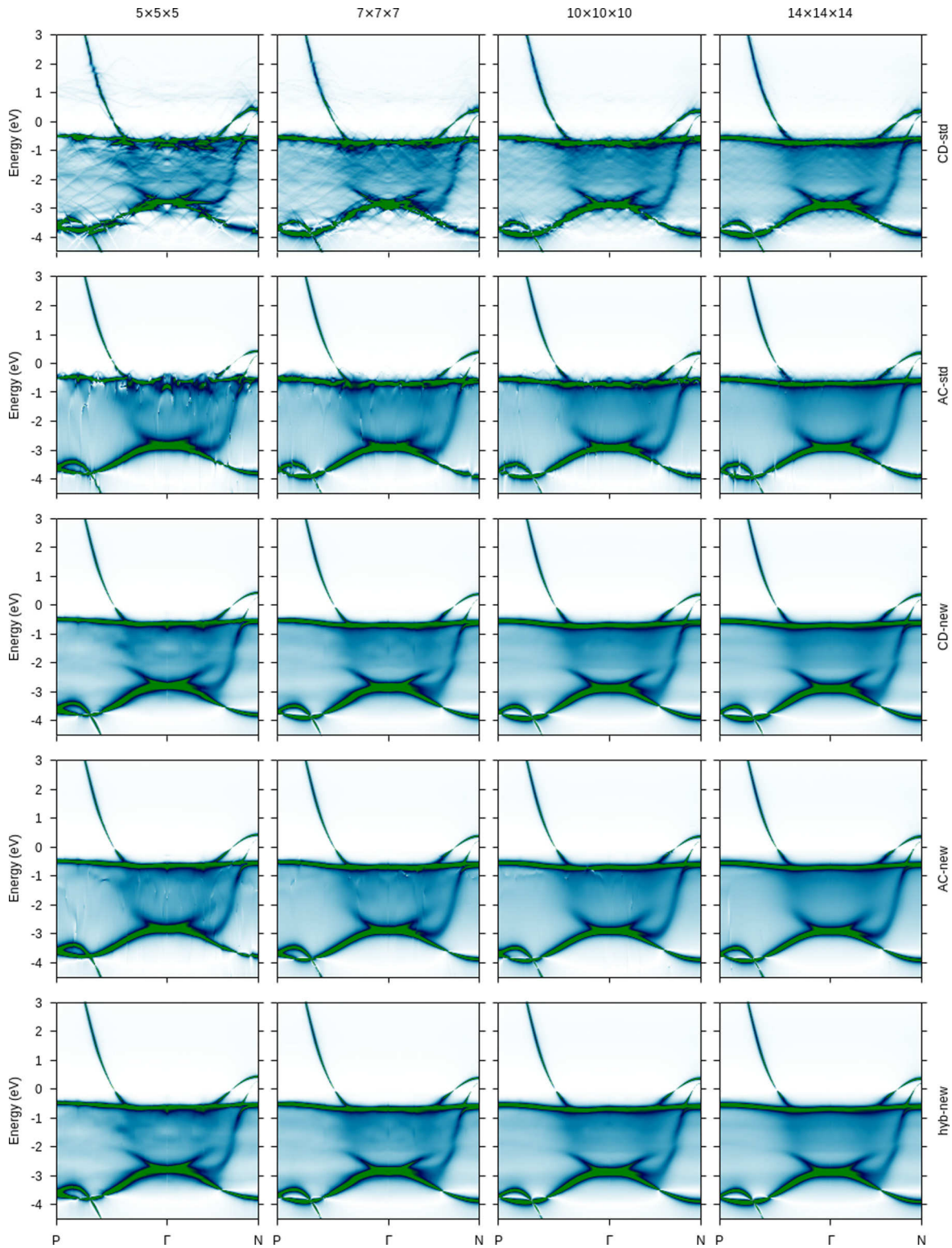

FIG. 7. *GT*-renormalized spin-up band structures of iron calculated with four methods: CD-std (standard tetrahedron method) (first row), AC-std (second row), CD-new (new tetrahedron method) (third row), AC-new (fourth row), and hyb-new (fifth row) as well as four **k**-point sets: $5 \times 5 \times 5$ (first column), $7 \times 7 \times 7$ (second column), $10 \times 10 \times 10$ (third column), and $14 \times 14 \times 14$ (fourth column).

The color plots enable a detailed investigation of the lifetime broadening.

The diagrams clearly demonstrate the numerical stability of the different techniques, which we abbreviate with CD-std, AC-std, CD-new, AC-new, and hyb-new, where "std" and "new" refer to the standard and new tetrahedron integrations, respectively. Given the strong variation of the self-energy seen in Fig. 5, it is surprising that CD-std yields a band structure, which, while clearly demonstrating numerical instabilities, is overall qualitatively correct. Although AC-std

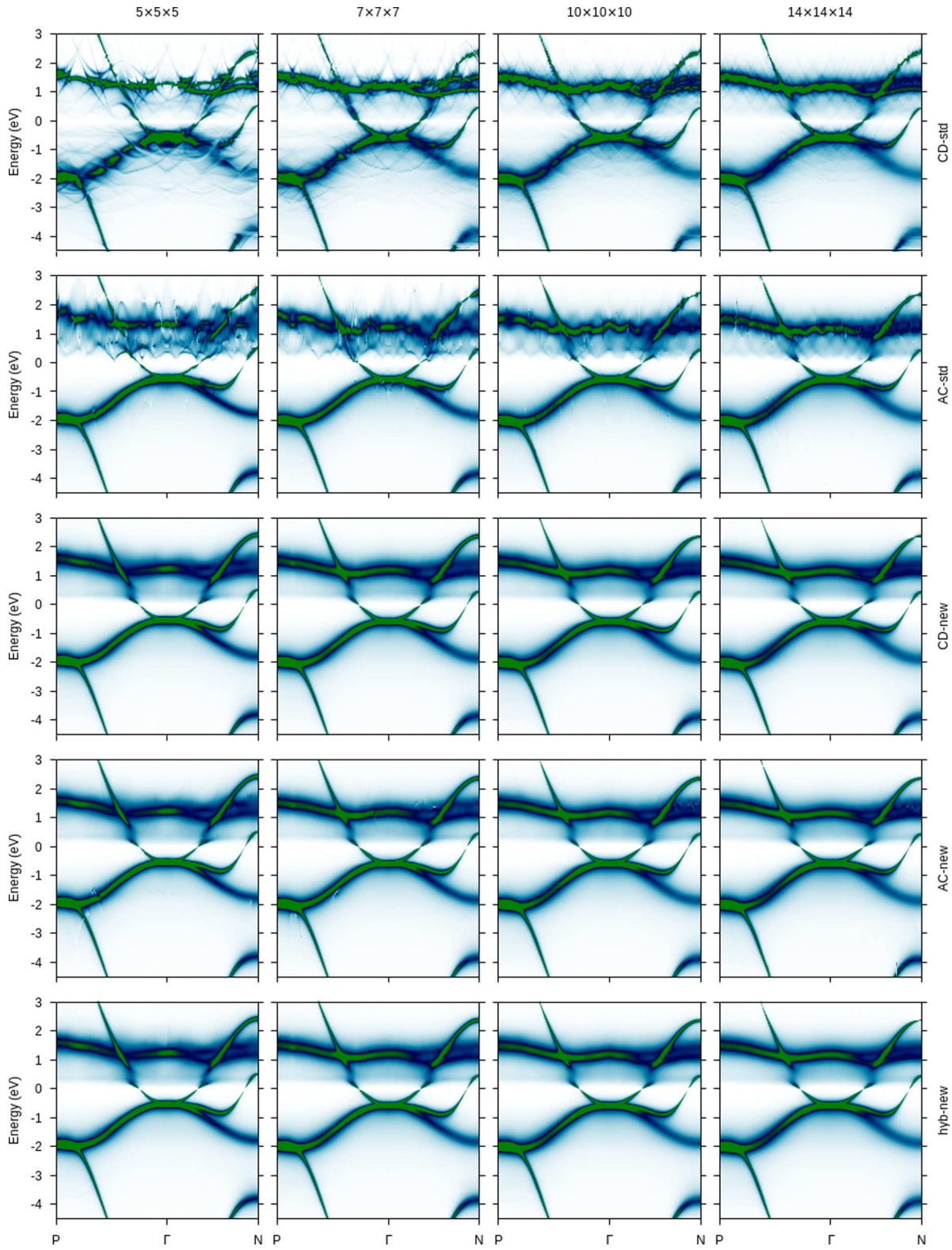

FIG. 8. Same as Fig. 7 for the spin-down channel.

improves on the quality of the band structure away from the Fermi energy due to the "smoothening" effect of the analytic continuation, the spurious oscillations of the self-energy [see Figs. 5(b) and 5(d)] worsen the accuracy of the spectral functions close to ϵ_F ($\omega = 0$). In principle, the instabilities can be "converged away" by improving the **k**-point sampling; the quality of the $14 \times 14 \times 14$ band structure is better than the one of the $5 \times 5 \times 5$ set. The convergence is, however, very slow, and the calculations soon become unwieldy.

The problems discussed above originate from using the standard tetrahedron method, which is not made for integrating highly nonlinear functions such as the T matrix. The

problems are solved with the new tetrahedron method as demonstrated by the *GT* band structures obtained from CD-new and AC-new. The CD-new plots are particularly smooth and show a very good **k**-point convergence. Even the diagram obtained with the coarsest **k**-point set $5 \times 5 \times 5$ differs only little from the one obtained with a $14 \times 14 \times 14$ **k**-point sampling. In the AC-new plots, one can see that the analytic continuation (extrapolation) from the imaginary to the real frequency axis introduces slight numerical instabilities in the band structures. These are more pronounced in the spin-up than in the spin-down channel because the many-body renormalization is stronger in the former. However, apart from these instabilities, the band structures obtained with CD-new and AC-new are very similar, while the computational time of the latter is much smaller than that of the former. In the last row, we have also included results from the *hybrid* method, which are (practically) identical to the ones from CD-new. The hybrid method is computationally faster than the CD technique, being between the CD and the AC method in terms of computational expense.

The high quality of the band structure plots now allow the many-body renormalization and lifetime broadening to be investigated in detail. A thorough investigation goes beyond the purpose of the present work and is deferred to another paper [6]. However, we want to point the attention of the reader to the strong renormalization effects seen for the occupied spin-up and unoccupied spin-down states. In the spin-up channel, the many-body effects lead to a loss of quasiparticle character in an energy range between -2.2 and -1.0 eV. This observation shows that an approximate solution of the quasiparticle equation as in standard *GW* calculations would be inappropriate for the present *GT* calculations, since the renormalized band structure cannot be described simply as a renormalized quasiparticle band structure with added lifetime effects. For example, the bands below -2.2 eV are clearly discernible, but, going up in energy, disappear due to the strong renormalization and, further up, reappear again. Furthermore, in the spin-down channel, two free-electron-like bands appear "interrupted" at around 0.5 eV above the Fermi energy. The spectral functions taken at the **q** momenta where the "energy gap" opens would exhibit a double peak structure, which clearly goes beyond a simple quasiparticle picture.

VI. CONCLUSIONS

In this paper, we have introduced a new tetrahedron integration technique that is made for the integration of highly-nonlinear functions in reciprocal space. It, thus, complements the standard tetrahedron method, which relies on the assumption that the integrand can be approximated as a linear function within the tetrahedra. The standard method replaces the integral over reciprocal space by a weighted sum over a finite set of **k** points. The new method, on the other hand, employs weight functions, defined for each state and **k** point. These weight functions are independent of the integrand and the integration bounds. They are smooth functions of frequency and, thus, allow integrating out any strong variations that the integrand may have.

The new method was applied to the *GT* self-energy, which contains the T matrix, a function that varies very strongly along the frequency axis due to the presence of sharp spin-wave resonances and a rich Stoner spectrum. As the T matrix enters the *GT* self-energy with the single-particle energies of the noninteracting reference system in its argument $[T(\omega - \epsilon^{\sigma}_{\mathbf{k}n})]$, the strong variation in frequency translates to an equally strong variation in reciprocal space.

It was shown that the new integration method substantially improves the quality of the self-energy and the numerical stability of the calculated renormalized band structure. In addition, it improves the **k**-point convergence considerably. Even **k**-point sets as coarse as $5 \times 5 \times 5$ yield iron band structures of very good quality. We presented results obtained with two general methods to evaluate the *GT* self-energy (which are also used for the *GW* approach): the contour-deformation technique and analytic continuation. Both approaches benefit substantially from the new tetrahedron **k** integration method. In addition, we have discussed a *hybrid* of the two methods, which gives (nearly) identical results to the standard contour-deformation approach, while being computationally cheaper.

The new tetrahedron method is not limited to the integration of self-energies. It can generally be applied for the integration of functions that vary strongly in reciprocal space (or, more precisely, that vary strongly with respect to a **k** dependent function, such as single-particle band energies), in particular, functions that represent excitation spectra, which can exhibit strong many-body resonances.

ACKNOWLEDGMENTS

The author thanks Irene Aguilera for a critical reading of the manuscript. Computing time granted through JARA-HPC on the supercomputer JURECA at Forschungszentrum Jülich is gratefully acknowledged.

APPENDIX A: INTEGRAL ALONG IMAGINARY FREQUENCY AXIS

When applying the new integration method to the first term of Eq. (27), an analytic evaluation of the integrals is possible as well. The derivation is however quite involved, which is why we discuss it here in detail. One would need to calculate

$$\frac{1}{2\pi}\int d\epsilon \int_{-\infty}^{\infty} d\omega' \frac{w_{\mathbf{k}}(\epsilon) T_{\mathbf{k}}(-\mathrm{i}\omega')}{\omega + \mathrm{i}\omega' - \epsilon} = \frac{1}{2\pi \mathrm{i}}\int d\epsilon \int_{-\infty}^{\infty} d\omega' \frac{w_{\mathbf{k}}(\epsilon) T_{\mathbf{k}}(-\mathrm{i}\omega')}{\omega' + \mathrm{i}(\epsilon - \omega)}, \tag{A1}$$

where we have omitted the indices n, m, and $\mathbf{q}$. Let us assume that $T(-z)$ is approximated according to Eq. (29) and let us consider only one term, i.e., $T(-\mathrm{i}\omega') \propto 1/(\mathrm{i}\omega' - p)$. The function $w_{\mathbf{k}}(\epsilon)$ is a third-order polynomial defined in intervals of ϵ. So, we have to calculate integrals of the type

$$\begin{aligned}\frac{1}{2\pi \mathrm{i}}\int_{\epsilon_1}^{\epsilon_2} d\epsilon\, \epsilon^m \int_0^{\infty} d\omega' \frac{1}{[\omega' + \mathrm{i}(\epsilon - \omega)](\mathrm{i}\omega' - p)} &= \frac{-1}{2\pi}\int_{\epsilon_1}^{\epsilon_2} d\epsilon\, \epsilon^m \int_0^{\infty} d\omega' \frac{1}{[\omega' + \mathrm{i}(\epsilon - \omega)](\omega' + \mathrm{i}p)} \\ &= \frac{1}{2\pi \mathrm{i}}\int_{\epsilon_1}^{\epsilon_2} d\epsilon\, \epsilon^m \frac{\ln[\mathrm{i}(\epsilon - \omega)] - \ln(\mathrm{i}p)}{\omega + p - \epsilon} =: \frac{I_m^{\omega,\epsilon_1,\epsilon_2}}{2\pi \mathrm{i}}\end{aligned} \tag{A2}$$

with $m = 0, 1, 2, 3$. (In the standard integration method, there is no ϵ integration, and the result is simply $\frac{1}{2\pi\mathrm{i}} \frac{\ln[\mathrm{i}(\epsilon-\omega)]-\ln(\mathrm{i}p)}{\omega+p-\epsilon}$ with $\epsilon = \epsilon_{\mathbf{k}n}$.)

With the help of $(1-x)^{-1} = \sum_{n=0}^{\infty} x^n$ and $\ln(1-x) = -\sum_{n=1}^{\infty} x^n/n$ for $|x| < 1$, three simple series expansions can be derived for the cases (a) $|\epsilon| < \min(|\omega+p|, |\omega|)$, (b) $|\epsilon-\omega| < |p|$, and (c) $|p| < |\epsilon-\omega|$ for all $\epsilon \in [\epsilon_1, \epsilon_2]$:

$$I_m^{\omega,\epsilon_1,\epsilon_2} = (\omega+p)^m \sum_{n=0}^{\infty} \frac{\ln(-\mathrm{i}\omega) - \ln(\mathrm{i}p) - \sum_{\nu=1}^{n}(1+p/\omega)^\nu/\nu}{n+m+1} \left(\frac{\epsilon}{\omega+p}\right)^{n+m+1}\Bigg|_{\epsilon_1}^{\epsilon_2} \quad \text{case(a)} \tag{A3}$$

$$I_m^{\omega,\epsilon_1,\epsilon_2} = \sum_{\mu=0}^{m} \binom{m}{\mu} \omega^{m-\mu} p^\mu \begin{cases} \sum_{n=\mu}^{\infty} J_n^{\omega,\epsilon_1,\epsilon_2}/p^{n+1} & \text{case (b)} \\ (-1)\sum_{n=1-\mu}^{\infty} p^{n-1} J_{-n}^{\omega,\epsilon_1,\epsilon_2} & \text{case (c)} \end{cases} \tag{A4}$$

with $J_n^{\omega,\epsilon_1,\epsilon_2} := J_n(\epsilon_2-\omega) - J_n(\epsilon_1-\omega)$ and

$$J_n(y) := \int y^n[\ln(y) - \ln(\mathrm{i}p)]dy = \begin{cases} \frac{1}{2}\ln(\mathrm{i}y)[\ln(\mathrm{i}y) - \ln(\mathrm{i}p)] & \text{for } n = -1 \\ \frac{y^{n+1}}{n+1}[\ln(\mathrm{i}y) - \ln(\mathrm{i}p) - \frac{1}{n+1}] & \text{for } n \neq -1 \end{cases}. \tag{A5}$$

Furthermore, a Taylor expansion with respect to $\epsilon_2 - \epsilon_1$ leads to

$$I_m^{\omega,\epsilon_1,\epsilon_2} = \sum_{n=0}^{\infty} \frac{(\epsilon_2-\epsilon_1)^{n+1}}{n+1} F_m^{(n)}(\epsilon_1) \tag{A6}$$

with

$$F_0^{(n)}(\epsilon) = \frac{1}{(\omega+p-\epsilon)^{n+1}} \left[\ln[-\mathrm{i}(\epsilon-\omega)] - \ln(\mathrm{i}p) + \sum_{\nu=1}^{n} \frac{(-1)^{\nu-1}}{\nu} \left(\frac{\omega+p-\epsilon}{\epsilon-\omega}\right)^\nu\right] \tag{A7}$$

and $F_m^{(n)}(\epsilon) = \epsilon F_{m-1}^{(n)}(\epsilon) + F_{m-1}^{(n-1)}(\epsilon)$ for $m > 0$. This Taylor expansion converges for $|\epsilon_2 - \epsilon_1| < \min(|\omega+p-\epsilon_1|, |\epsilon_1 - \omega|)$. There is an analogous Taylor expansion around ϵ_2.

These power series already cover most of the situations. However, for the case that neither of the above conditions (which should be made stricter for numerical reasons) are fulfilled, we need to derive an exact analytic expression for the integral in Eq. (A2). Later, we will also have to consider the case of a branch cut. We note in passing that the power series converge very quickly where the analytic expression to be derived in the following becomes numerically unstable.

As a first remark, one might be tempted to replace the numerator by $\ln(\epsilon-\omega) - \ln(p)$ or even $\ln(\frac{\epsilon-\omega}{p})$ using $\ln(ab) = \ln(a) + \ln(b)$, but this latter relationship is only valid modulo $2\pi\mathrm{i}$ in the case of complex logarithms: $\ln(ab) - \ln(a) - \ln(b)$ can take the three values 0, $2\pi\mathrm{i}$, and $-2\pi\mathrm{i}$. As a second important remark, the primitive of $1/z$ is not unique. Instead of $\ln(z)$ one can choose $\ln(az)$ with any nonzero complex number a [as is easily proven by differentiating $\ln(az)$]. The choice of a (to be more precise, its phase) affects the location of the branch cut. Here, we take $\ln(z)$ as the primitive because the value at the upper bound $\lim_{\omega'\to\infty} \ln[\omega' + \mathrm{i}(\epsilon-\omega)] - \ln(\omega' + \mathrm{i}p)$ then disappears.

For $m = 0$, we substitute $t = \frac{\epsilon-\omega}{p}$ and get

$$\begin{aligned} I_0^{\omega,\epsilon_1,\epsilon_2} &= \int_{t_1}^{t_2} dt\, \frac{\ln(\mathrm{i}pt) - \ln(\mathrm{i}p)}{1-t} \\ &= [\ln(\mathrm{i}p) - \ln(\mathrm{i}pt)]\ln(1-t) - \mathrm{Li}_2(1-t)\Big|_{t_1}^{t_2} \\ &= \{\ln(\mathrm{i}p) - \ln[\mathrm{i}(\epsilon-\omega)]\}\ln\left(1 - \frac{\epsilon-\omega}{p}\right) \\ &\quad - \mathrm{Li}_2\left(1 - \frac{\epsilon-\omega}{p}\right)\Big|_{\epsilon_1}^{\epsilon_2} \end{aligned} \tag{A8}$$

with the dilogarithm $\mathrm{Li}_2(z) = \int_1^z \frac{\ln(t)}{1-t}dt$ (Spence's function), see Appendix B. It is instructive to consider the incorrect usage of $\ln(\mathrm{i}pt) - \ln(\mathrm{i}p) = \ln(t)$, which would lead to the much simpler but incorrect result $\mathrm{Li}_2(t)$. There is a relationship between $\mathrm{Li}_2(t)$ and $\mathrm{Li}_2(1-t)$ (Appendix B), which turns the above expression into $\mathrm{Li}_2(t) + [\ln(\mathrm{i}p) + \ln(t) - \ln(\mathrm{i}pt)]\ln(1-t) - \frac{\pi^2}{6}$. The second term (the constant third term is irrelevant for the primitive) corrects for the fact that $\ln(\mathrm{i}p) + \ln(t) - \ln(\mathrm{i}pt)$ can be a multiple of $2\pi\mathrm{i}$. Differentiating this expression gives $\frac{\ln(t)+[\ln(\mathrm{i}pt)-\ln(t)-\ln(\mathrm{i}p)]}{1-t}$, the bracket $[\ldots]$ taking care of the multivaluedness.

For $m > 0$, we can use the recursion

$$\begin{aligned} I_m^{\omega,\epsilon_1,\epsilon_2} &:= \int_{\epsilon_1}^{\epsilon_2} d\epsilon\, \epsilon^m \frac{\ln[\mathrm{i}(\epsilon-\omega)] - \ln(\mathrm{i}p)}{\omega+p-\epsilon} \\ &= \int_{\epsilon_1}^{\epsilon_2} d\epsilon\, \epsilon^{m-1}[\ln[\mathrm{i}(\epsilon-\omega)] \\ &\quad - \ln(\mathrm{i}p)]\left(\frac{\omega+p}{\omega+p-\epsilon} - 1\right) \\ &= \ln(\mathrm{i}p)\frac{\epsilon^m}{m}\Big|_{\epsilon_1}^{\epsilon_2} + (\omega+p)I_{m-1}^{\omega,\epsilon_1,\epsilon_2} - L_{m-1}^{\omega,\epsilon_1,\epsilon_2}, \end{aligned} \tag{A9}$$

where $L_m^{\omega,\epsilon_1,\epsilon_2} = \int_{\epsilon_1}^{\epsilon_2} \epsilon^m \ln[\mathrm{i}(\epsilon-\omega)]d\epsilon = \sum_{\mu=0}^{m} \binom{m}{\mu}\omega^{m-\mu}(-1)^\mu\{l_\mu[\mathrm{i}(\epsilon_2-\omega)] - l_\mu[\mathrm{i}(\epsilon_1-\omega)]\}$ and $l_\mu(t) = \int t^\mu \ln t dt = \frac{t^{\mu+1}}{\mu+1}[\ln(t) - \frac{1}{\mu+1}]$ for $\mu \geqslant 0$.

One has to take into account the branch cuts of the primitive in Eq. (A8). The branch cuts of the functions $\ln(z)$ and $\mathrm{Li}_2(z)$ are along the negative real axis. Let us assume that the argument $1-t$ crosses this axis at $1-t_0 < 0$. The dilogarithm $\mathrm{Li}_2(1-t_0)$ changes value there by $-2\pi\mathrm{i}\ln(t_0)$ (crossing the real axis from above). With $\ln(\mathrm{i}p) - \ln(\mathrm{i}pt_0) = -\ln(t_0)$

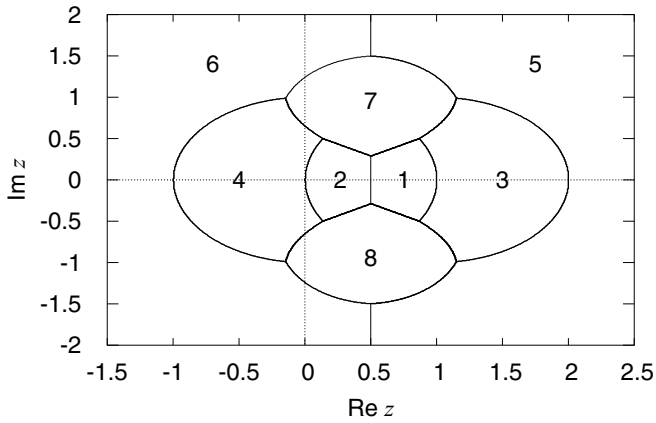

FIG. 9. Complex plane with numbers (1–8) labeling the regions where the respective series for the dilogarithm $\mathrm{Li}_2(z)$ converges fastest (see text).

(which holds true in this case as t_0 is a real positive number), one obtains the same step for the other term, canceling the first step exactly. So, for the argument $1-t$, there is no problem with the branch cut. However, if the branch cut of $\ln(\mathrm{i}pt)$ is crossed by the integration path, i.e., if there is a t_0 along the path $[t_1, t_2]$ that fulfills $\Re(pt_0) = 0$ and $\Im(pt_0) > 0$, we define $I_m^{\omega,\epsilon_1,\epsilon_2} := I_m^{\omega,\epsilon_1,\epsilon_0\mp\eta} + I_m^{\omega,\epsilon_0\pm\eta,\epsilon_2}$ for $\epsilon_1 \lessgtr \epsilon_2$ and $\epsilon_0 = \Re\omega$ (following from $\Re(\epsilon_0 - \omega) = \Re(pt_0) = 0$) with a positive infinitesimal η.

For the negative integral branch (from $-\infty$ to 0), we first assume the symmetry $T(\mathrm{i}\omega) = T(-\mathrm{i}\omega)$ (which is fulfilled by W but actually *not* by the T matrix, see below), so $T(\mathrm{i}\omega') \propto 1/(\mathrm{i}\omega' - p)$ as before. Then, the negative integral branch contributes with

$$\begin{aligned}
&\frac{1}{2\pi\mathrm{i}}\int_{\epsilon_1}^{\epsilon_2} d\epsilon\,\epsilon^m \int_{-\infty}^{0} d\omega' \frac{1}{[\omega' + \mathrm{i}(\epsilon-\omega)](-\mathrm{i}\omega' - p)} \\
&= \frac{1}{2\pi}\int_{\epsilon_1}^{\epsilon_2} d\epsilon\,\epsilon^m \int_{-\infty}^{0} d\omega' \frac{1}{[\omega' + \mathrm{i}(\epsilon-\omega)](\omega' - \mathrm{i}p)} \\
&= \frac{1}{2\pi\mathrm{i}}\int_{\epsilon_1}^{\epsilon_2} d\epsilon\,\epsilon^m \frac{\ln[-\mathrm{i}(\epsilon-\omega)] - \ln(\mathrm{i}p)}{-\omega + p + \epsilon} \\
&= \frac{(-1)^m}{2\pi\mathrm{i}}\int_{-\epsilon_1}^{-\epsilon_2} d\epsilon\,\epsilon^m \frac{\ln[\mathrm{i}(\epsilon+\omega)] - \ln(\mathrm{i}p)}{-\omega + p - \epsilon} \\
&= \frac{(-1)^m}{2\pi\mathrm{i}} I_m^{-\omega,-\epsilon_1,-\epsilon_2},
\end{aligned} \tag{A10}$$

where we have taken $\ln(-z)$ as the primitive of $1/z$ because the integration now extends to $-\infty$. Obviously, we simply have to replace $\epsilon_1, \epsilon_2, \omega \to -\epsilon_1, -\epsilon_2, -\omega$ and can then use the same formulas as before. If $T(\mathrm{i}\omega) \neq T(-\mathrm{i}\omega)$, one would have to determine the poles and residues of the Padé formula specifically for $T(\mathrm{i}\omega)$ and evaluate Eq. (A10) with these new parameters. For example, for the T matrix, we have the symmetry $T(\mathrm{i}\omega) = T^*(-\mathrm{i}\omega)$, whence $a_\mu \to -a_\mu^*$ and $p_\mu \to -p_\mu^*$.

We note that the tetrahedron weight functions should be defined as polynomials with respect to a relative energy such as $\epsilon - \epsilon_{\mathbf{k}n}$, as recommended in Sec. II B. It is easy to see that the above formulas remain valid if we set $\epsilon \to \epsilon - \epsilon_{\mathbf{k}n}$ and $\omega \to \omega - \epsilon_{\mathbf{k}n}$.

APPENDIX B: DILOGARITHM (SPENCE'S FUNCTION)

The dilogarithm (Spence's function) is defined by

$$\mathrm{Li}_2(z) := \int_1^z \frac{\ln(t)}{1-t} dt\,. \tag{B1}$$

The argument z can be complex, and $\mathrm{Li}_2(z)$ has a branch cut at $(-\infty, 0)$. The dilogarithm is given by the series expansion

$$\mathrm{Li}_2(z) = \sum_{\mu=1}^{\infty} \frac{(1-z)^\mu}{\mu^2} \tag{B2}$$

for $|1-z| \leqslant 1$ (series 1 of Fig. 9). Note that $\ln(z)$ has a similar series with the denominator μ, hence the name. The dilogarithm fulfills the identities

$$\mathrm{Li}_2(1-z) = -\int_0^z \frac{\ln(1-t)}{t} dt = \int_0^z \left[-\frac{\ln(1-t)}{t} + \frac{\ln(t)}{1-t}\right] dt - \mathrm{Li}_2(z) + \frac{\pi^2}{6} = -\mathrm{Li}_2(z) - \ln(z)\ln(1-z) + \frac{\pi^2}{6}, \tag{B3}$$

$$\mathrm{Li}_2\left(\frac{1}{z}\right) = \int_1^{1/z} \frac{\ln(t)}{1-t} dt = \int_1^z \frac{\ln(s)}{1-\frac{1}{s}} \frac{ds}{s^2} = \int_1^z \ln(s)\left(\frac{1}{s-1} - \frac{1}{s}\right) ds = -\mathrm{Li}_2(z) - \frac{1}{2}\ln^2(z)\,, \tag{B4}$$

and a special value is $\mathrm{Li}_2(0) = \sum_{\mu=1}^{\infty} 1/\mu^2 = \pi^2/6$. With the help of these identities one can relate $\mathrm{Li}_2(z)$ to $\mathrm{Li}_2(y)$ with $y = 1-z$, $\frac{1}{z}$, $\frac{1}{1-z}$, $1-\frac{1}{z}$, and $\frac{1}{1-\frac{1}{z}}$ (series 2–6), which allows to pick that y for which the series converges most quickly, i.e., for which $|1-y|$ is minimal (and smaller than 1). The resulting series converge quickly except for (the neighborhood of) $q = 1/2 + \mathrm{i}\sqrt{3}/2$ ($|q| = 1$) and q^*. The numbers 0, 1, q (and 0, 1, q^*) form an equilaterial triangle on the complex plane. For these two points, we have $\mathrm{Li}_2(q) = \frac{\pi^2}{36} + \mathrm{i}V_0$ and $\mathrm{Li}_2(q^*) = \mathrm{Li}_2^*(q)$ with the Gieseking constant $V_0 = 1.0149416(\ldots)$. For the neighborhood of q, we find

$$\begin{aligned}
\mathrm{Li}_2(q+x) &= \mathrm{Li}_2(q) + \int_0^x \frac{\ln(q+s)}{q^*-s} ds = \mathrm{Li}_2(q) + \int_0^x \frac{\mathrm{i}\frac{\pi}{3} + \ln(1+s/q)}{q^*-s} ds \\
&= \mathrm{Li}_2(q) + \mathrm{i}\frac{\pi}{3}[\ln(q^*) - \ln(q^*-x)] + \int_0^{x/q^*} \frac{\ln(1-qy)}{1-y} dy\,,
\end{aligned} \tag{B5}$$

where we have used that $\ln(q) = i\pi/3$ and $q^*/q = -q$ as well as the fact that $\ln(q+s) = \ln(q) + \ln(1+s/q)$ is valid because $q(1+s/q)$ does not cross a branch cut of $\ln(z)$ along the s integration path (x is a small parameter). The last term can be written as a series

$$\begin{aligned}\int \frac{\ln(1-qy)}{1-y}dy &= -\sum_{m=1}^{\infty}\frac{q^m}{m}\int \frac{y^m}{1-y}dy = -\sum_{m=1}^{\infty}\frac{q^m}{m}\left[-\ln(1-y) - \sum_{\mu=1}^{m}\frac{y^\mu}{\mu}\right] \\ &= -\ln(1-q)\ln(1-y) + \sum_{m=1}^{\infty}\frac{q^m}{m}\sum_{\mu=1}^{m}\frac{y^\mu}{\mu} \\ &= -\ln(1-q)\ln(1-y) + \sum_{\mu=1}^{\infty}\frac{y^\mu}{\mu}\sum_{m=\mu}^{\infty}\frac{q^m}{m} \\ &= -\ln(1-q)\ln(1-y) + \sum_{\mu=1}^{\infty}\frac{y^\mu}{\mu}\left[-\ln(1-q) - \sum_{m=1}^{\mu-1}\frac{q^m}{m}\right] \\ &= -\sum_{\mu=2}^{\infty}\frac{y^\mu}{\mu}\left(\sum_{m=1}^{\mu-1}\frac{q^m}{m}\right) \end{aligned} \tag{B6}$$

as one can easily verify by differentiating both sides. Now we use $1/q^* = q$ and the fact that $\ln(q^*) - \ln(q^*-x) = -\ln(1-\frac{x}{q^*})$ is valid because the product $q(q^*-x)$ does not cross the branch cut of $\ln(z)$ and obtain

$$\begin{aligned}\mathrm{Li}_2(q+x) &= \mathrm{Li}_2(q) + i\frac{\pi}{3}[\ln(q^*) - \ln(q^*-x)] - \sum_{\mu=2}^{\infty}\frac{(xq)^\mu}{\mu}\left(\sum_{m=1}^{\mu-1}\frac{q^m}{m}\right) \\ &= \mathrm{Li}_2(q) - i\frac{\pi}{3}\ln\left(1-\frac{x}{q^*}\right) - \sum_{\mu=2}^{\infty}\frac{(xq)^\mu}{\mu}\left(\sum_{m=1}^{\mu-1}\frac{q^m}{m}\right)\end{aligned} \tag{B7}$$

(series 7), where the double sum in the last term can be implemented in a single loop. One can also express Eq. (B7) as

$$\mathrm{Li}_2(z) = \mathrm{Li}_2(q) + \frac{\pi}{3}\left[\frac{\pi}{3} - i\ln(1-z)\right] - \sum_{\mu=2}^{\infty}(z-q)^\mu\frac{q^\mu}{\mu}\left(\sum_{m=1}^{\mu-1}\frac{q^m}{m}\right). \tag{B8}$$

For $\mathrm{Li}_2(q^*+x)$, we use $\mathrm{Li}_2(q^*+x) = \mathrm{Li}_2^*(q+x^*)$ (series 8).

[1] F. Bloch, Z. Phys. **61**, 206 (1930).
[2] H. J. Monkhorst and J. D. Pack, Phys. Rev. B **13**, 5188 (1976).
[3] J. Rath and A. Freeman, Phys. Rev. B **11**, 2109 (1975).
[4] L. Hedin, Phys. Rev. **139**, A796 (1965).
[5] M. Springer, F. Aryasetiawan, and K. Karlsson, Phys. Rev. Lett. **80**, 2389 (1998).
[6] M. C. T. D. Müller, S. Blügel, and C. Friedrich, Phys. Rev. B **100**, 045130 (2019).
[7] P. E. Blöchl, O. Jepsen, and O. K. Andersen, Phys. Rev. B **49**, 16223 (1994).
[8] C. Friedrich, S. Blügel, and A. Schindlmayr, Phys. Rev. B **81**, 125102 (2010).
[9] H. N. Rojas, R. W. Godby, and R. J. Needs, Phys. Rev. Lett. **74**, 1827 (1995).
[10] M. M. Rieger, L. Steinbeck, I. White, H. Rojas, and R. Godby, Comput. Phys. Commun. **117**, 211 (1999).
[11] R. W. Godby, M. Schlüter, and L. J. Sham, Phys. Rev. B **37**, 10159 (1988).
[12] F. Aryasetiawan, *Electronic Structure Calculations in Advances in Condensed Matter Science* (Gordon and Breach, New York, 2000).
[13] *Pade approximants*, edited by G. A. Baker and P. Graves-Morris, 2nd ed. Encyclopedia of Mathematics and its Applications (Cambridge University Press, Cambridge, 1996).
[14] G. E. Engel, B. Farid, C. M. M. Nex, and N. H. March, Phys. Rev. B **44**, 13356 (1991).
[15] D. Krause and P. Thörnig, J. Large-Scale Res. Fac. **4**, A132 (2019).